Journal of Hydrology 568 (2019) 658–675

Contents lists available at ScienceDirect

Journal of Hydrology

journal homepage: www.elsevier.com/locate/jhydrol

Research papers

Typhoon-induced changes in rainfall interception loss from a tropical multi-species 'reforest'

Jun Zhang[a,b,*], L. Adrian Bruijnzeel[c,d], H.J. (Ilja) van Meerveld[e], Chandra P. Ghimire[f], Roger Tripoli[g], Arturo Pasa[g], John Herbohn[d]

[a] Faculty of Science, VU University, De Boelelaan 1085, 1081 HV Amsterdam, the Netherlands
[b] College of Hydrology and Water Resources, Hohai University, Nanjing, Jiangsu, People's Republic of China
[c] Department of Geography, King's College London, London, United Kingdom
[d] Tropical Forests and People Research Centre, University of the Sunshine Coast, Maroochydore, Queensland, Australia
[e] Department of Geography, Hydrology and Climate, University of Zurich, Zurich, Switzerland
[f] AgResearch, Lincoln Research Centre, Private Bag 4749, Christchurch 8140, New Zealand
[g] ACIAR Smallholder Forestry Project, Visayas State University, Baybay City, Leyte, Philippines

ARTICLE INFO

This manuscript was handled by Marco Borga, Editor-in-Chief, with the assistance of Patrick Norman Lane, Associate Editor

Keywords:
Leaf area index
Leyte Island
Reforestation
Stemflow
Throughfall
Wet-canopy evaporation

ABSTRACT

Typhoon Haiyan made landfall in the central Philippines on 8 November 2013 as one of the strongest tropical cyclones ever. It also affected a 23-year-old multi-species 'reforest' at Manobo near Tacloban City on Leyte Island. As part of a larger hydrological investigation of the impacts of reforestation on streamflow response in the Tacloban area, gross rainfall (*P*), throughfall (TF; 24 roving collectors) and stemflow (SF; 12 trees) were monitored at Manobo between June 2013 and May 2014. Leaf Area Index (LAI) above each TF collector was measured regularly. Total rainfall interception losses (*I*) were determined using Gash's revised analytical model for three consecutive periods:(i) pre-Haiyan (baseline), (ii) post–Haiyan (damaged canopy), and (iii) after initial canopy recovery. Modeled *I* was 18% of *P* before disturbance, 12% for the period with the most extensive canopy damage, and 17.5% after initial canopy recovery. Stemflow was low, and weighted mean values accounted for 2.7%, 1.3% and 2.0% of *P* for the respective periods. Contrasts in period-average values of *I* reflected changes in LAI as well as wet-canopy evaporation rates. Storm-based TF fractions at the 5 m × 5 m sub-plot scale were inversely related to LAI, especially for small storms and low rainfall intensities. Inferred hourly rates of wet-canopy evaporation showed a strong positive relationship to hourly rainfall intensity during large storms. The revised analytical model was also run using pre-disturbance parameter values for the entire year to assess the overall effect of canopy damage on *I*. Estimated annual losses with and without canopy disturbance were 514 mm (15% of *P*) and 572 mm (17%), respectively. Thus, observed and inferred changes in rainfall partitioning after canopy disturbance and initial recovery were comparatively modest, likely because the measurement site was relatively sheltered from the winds during typhoon passage and re-foliation relatively rapid. However, given the predicted increase in occurrence of 'super-typhoons' due to continued global warming and oceanic freshening, the structure of forests in affected regions can be expected to be modified, with potential consequences for rainfall partitioning and hydrological response.

1. Introduction

The natural succession of the vegetation in humid tropical areas subject to intensifying slash-and-burn cultivation is often arrested by repeated fire, and so-called fire-climax grasslands tend to form instead (Garrity et al., 1997; Hooper et al., 2005; Styger et al., 2007). Soils associated with these *Imperata*- and *Saccharum*-dominated grasslands can be physically and chemically degraded, rendering them relatively unproductive (Ohta, 1990; Santoso et al., 1997) and prone to overland flow generation (Chandler and Walter, 1998; Zhang et al., 2018a, b) and surface erosion, especially when grazed (Concepcion and Samar, 1995; Snelder, 2001; Ziegler et al., 2009). In response to these problems, fire-climax grasslands across the tropics are being targeted increasingly for conversion to more productive and environmentally favourable forms of land use, such as reforestation and agroforestry (Otsamo et al., 1997; Murniati, 2002; Wishnie et al., 2007; Snelder and

* Corresponding author at: Room E-260, Faculty of Science, VU University, De Boelelaan 1085, 1081 HV Amsterdam, the Netherlands.
E-mail address: jzg290@outlook.com (J. Zhang).

https://doi.org/10.1016/j.jhydrol.2018.11.024
Received 18 August 2017; Received in revised form 17 October 2018; Accepted 7 November 2018
Available online 17 November 2018
0022-1694/

Lasco, 2008; Ancog et al., 2016). Although the harsh environmental conditions and recurring fires typically associated with these grasslands tend to preclude the natural re-establishment of forest, the grasses can be shaded out by planting fast-growing tree species in combination with intensive initial site management (Otsamo, 2000; Murniati, 2002). The associated improvements in below-canopy micro-climatic conditions reduce the competitive ability of the grasses and promote the germination and development of native tree seedlings, resulting in mixed stands with the planted (usually exotic) species dominating the main canopy and naturally regenerating native species being dominant in the understory (Lamb, 1998; Otsamo, 2000; cf. Wills et al., 2016). Thus, although upon maturation the resulting forest neither classifies as a pure plantation nor as fully naturally developed secondary forest, a multi-species ecosystem is created that may be appropriately called a 'reforest' (Chazdon et al., 2016). Secondary forests and reforests in various stages of growth constitute the dominant forest type nowadays in many humid tropical regions (FAO, 2010; Chazdon, 2014). Yet, our understanding of the associated changes in hydrological functioning (Hölscher et al., 2005; Ziegler et al., 2009; Dierick et al., 2010; Zimmermann et al., 2013) as well as their impact on streamflow (Beck et al., 2013; Lacombe et al., 2016) remains limited.

The Philippines, where *Imperata* grasslands are referred to as *cogon*, represents a case in point. Due to heavy logging and decades of slash-and-burn cultivation, nearly 60% (9.3 Mha) of all land officially designated to be under forest is actually without trees (including up to 5 Mha of *cogon*; Garrity et al., 1997; Lasco and Pulhin, 2006) and in need of ecological rehabilitation (Pulhin et al., 2006; Asio et al., 2009). The country launched an ambitious 'National Greening Program' in 2011, targeting the planting of trees on 1.5 million ha of degraded land, much of it *cogon* (Aquino and Daquio, 2014). According to FAO (2016), the Philippines reforested 240,000 ha between 2010 and 2015, thus reversing the net loss of forest cover in the previous years to a net gain. Although tree planting on grass- and shrubland has generally resulted in decreases in water yield world-wide (Farley et al., 2005; Ford et al., 2011; Lacombe et al., 2016), claims of a positive effect on dry-season flows are occasionally reported (Zhou et al., 2010; Krishnaswamy et al., 2012; cf. Scott et al., 2005). As part of an investigation into a similar claim that formerly ephemeral streamflow became perennial about seven to eight years after reforesting *cogon* grassland in north-eastern Leyte Island (the Philippines) (U. Padecio, personal communication), we measured rainfall interception losses (I) between June 2013 and May 2014 in the 23-year-old community-managed Manobo reforest near Tacloban City. Values of I for semi-mature (10–25 years old) secondary tropical forests are often already indistinguishable from those reported for old-growth forests (e.g. Hölscher et al., 1998; Macinnis-Ng et al., 2012; Zimmermann et al., 2013). Moreover, average I from tropical forests subject to 'maritime' climatic conditions (like those prevailing in the Philippines) tends to be roughly twice that inferred for forests at mid-continental locations (Roberts et al., 2005; Wallace and McJannet, 2008). While the reasons for this contrast are debated in terms of the exact mechanisms involved and the sources of the non-radiant energy required to sustain such high rates of evaporation (see discussion in Holwerda et al. (2012) and Van Dijk et al. (2015)), the impact of the high I observed for 'maritime' tropical forests on the overall water budget is potentially large (McJannet et al., 2007; cf. Roberts et al., 2005).

The Philippine region experiences 6–9 tropical cyclone passages on average per year (Cinco et al., 2016) and on 8 November 2013 the Manobo reforest was hit by one of the strongest and most devastating events on record (super-typhoon Haiyan – locally called Yolanda; Nguyen et al., 2014; Rabonza et al., 2015). It also affected the Manobo reforest. This presented an opportunity to study the changes in I associated with: (i) intensive forest disturbance and damage; and (ii) subsequent (partial) canopy recovery. Despite the expected increase in general typhoon strength (Knutson et al., 2010; Kossin et al., 2014) and the frequency of 'super-typhoons' in particular due to global warming-induced upper-oceanic freshening (Balaguru et al., 2016), studies of the effects of tropical forest disturbance by extreme winds (as opposed to gap creation by selective logging; Asdak et al., 1998b; Chappell et al., 2001) on the magnitude of I are comparatively rare (Scatena et al., 1996; Waterloo et al., 1999; Heartsill-Scalley et al., 2007). The effect has been shown to last up to a year, depending on the degree of canopy disturbance and the rate of re-foliation (Scatena et al., 1996; Waterloo, 1994; Hu and Smith, 2018). Point measurements of canopy drip in intact tropical forests have also been shown to be inversely related to the density of the canopy overhead (Burghouts et al., 1998; Fleischbein et al., 2005; Holwerda, 2005; Zimmermann et al., 2013). We therefore hypothesized a strong initial decrease in I after opening up of the forest canopy by typhoon Haiyan, followed by a gradual return to pre-disturbance values as the forest's foliage recovered (cf. Heartsill-Scalley et al., 2007).

2. Study area

The Manobo reforest (11°17′N, 124°56′E) is located 8 km northwest of Leyte's capital city Tacloban and 1.8 km from the Pacific Ocean in the East. Elevations range between 33 and 220 m a.s.l. The study site within the 8.75 ha catchment, where the interception measurements were conducted, was at an elevation of ~110 m a.s.l. on a steep SW-orientated hillslope (gradient 25–30°). The climate is tropical ever-wet (type Af according to the Köppen-Geiger classification) without a clearly developed dry season. Mean annual precipitation measured at Tacloban Airport (3 m a.s.l.; 11 km from the Manobo site) between 1977 and 2011 (PAGASA Office, Tacloban) was 2660 mm (195 rain days with ≥0.5 mm of rain each) with high inter-annual variability (range: 1435–4790 mm). The regional climate is affected by the El Niño Southern Oscillation (ENSO) phenomenon, such that (strong) ENSO events usually cause severe drought (Thirumalai et al., 2017; cf. Fig. 3a). As illustrated by the high variability in rainfall amounts observed for wet-season months shown in Fig. 3b below, wet-season rainfall depends on the strength of the monsoon and the number of tropical storms and cyclones (typhoons) passing through the Philippine archipelago (Cinco et al., 2016). On average, five out of 12 months have more than 200 mm of rain each at Tacloban (classifying them as 'very wet': October–February; Fig. 3b), while the remaining seven months receive on average more than 100 mm each ('wet'), yielding a value of 17 (out of 24) for the Walsh (1996) climatic per-humidity index (PI). April is the driest month usually (average rainfall: 127 mm; range: 20–620 mm) and December the wettest (378 mm on average; range: 90–782; Fig. 3b). Rainfall at Tacloban is delivered mostly in the form of relatively small events (50% of all rain days (defined as having ≥0.1 mm) receive < 5 mm and 67% < 10 mm), but due to its location close to the north-eastern coastline of Leyte Island (facing the Western Pacific Basin, one of the world's premier tropical cyclone generating areas; García-Herrera et al., 2007; cf. de Gouvenain and Silander, 2003) the study area receives about 30% of its annual rainfall from tropical cyclones and depressions (Cinco et al., 2016). Mean monthly temperatures at Tacloban range from 25.7 °C in January to 28.1 °C in May, while seasonal variation in average daily relative humidity is small (81–86%). Average monthly wind speeds at Tacloban vary between 1.5 and 2.4 m s^{-1}, but instantaneous wind speeds can be very high (as during typhoon passage; cf. García-Herrera et al., 2007; Cinco et al., 2016). Average daily reference evaporation (Allen et al., 1998) computed from basic climatic data for Tacloban Airport ranges between 3.0 mm d^{-1} (December) and 4.8 mm d^{-1} (April).

The study forest is underlain by mafic rocks (gabbro) of the Tacloban ophiolite complex (Dimantala et al., 2006) in which Eutric Cambisols (FAO, 2006) with a sandy clay loam texture have developed. Prior to the mid-1980s, the area consisted of regularly burned *cogon* grassland. From 1990 onwards, members of the displaced Manobo tribe began planting large numbers of beech wood (*Gmelina arborea* Roxb.), mahogany (*Swietenia macrophylla* King) and, to a lesser extent (< 5%)

Table 1
Comparative structural characteristics for the three forest plots at Manobo. Interception measurements were conducted in the middle plot only.

Plot	Tree density (ha^{-1})	Tree height (m)	DBH (cm)	Crown area (m^2)	Basal area (m^2 ha^{-1})	LAI	Species
Lower	1600	6.6 ± 2.3	10.4 ± 8.0	16.3 ± 15.0	13.6	4.0 ± 0.7[#]	27
Middle	1367	7.6 ± 2.5	10.8 ± 6.6	14.5 ± 11.8	12.5	4.8 ± 1.2[+]	27
Upper	2277	7.4 ± 2.4	9.6 ± 5.0	9.4 ± 12.2	16.5	5.7 ± 0.7[*]	29

[#] As measured along central contour of plot on 26 August 2013
[+] Idem, mean for 7 June and 26 August 2013.
[*] Idem on 7 June 2013.

coconut palm trees (*Cocos nucifera* L.) to shade out the *Imperata* grass. Subsequently, rattans (*Calamus spp*.) and various medicinal plants were added (U. Padecio, personal communication). At the start of the study (June 2013), the 23-year-old forest consisted of a mixture of these planted trees and numerous naturally regenerating tree species. Average canopy height (determined in May 2013 for an area of 1850 m^2 that included a lower (60 m × 10 m at 80 m a.s.l., SW aspect), middle (idem at 110 m a.s.l., SW aspect) and upper (65 m × 10 m at 145 m a.s.l., SE aspect) plot) was 7.3 ± 2.4 (SD) m (range 1.9–16.0 m). Average diameter at breast height (DBH) for all 324 trees with DBH ≥ 5 cm was 10.5 ± 6.6 cm, representing an overall basal area of 15.3 m^2 ha^{-1} (range 12.5–16.5 m^2 ha^{-1}). Table 1 summarizes the basic structural characteristics of the three plots, indicating no clear trends with slope position other than a (slight) decrease in average projected crown area (but not tree height, DBH nor basal area) in a downslope direction. Based on its intermediate values for LAI (Table 1) and mean projected crown area, as well as its mid-slope position, the middle forest plot was chosen for the rainfall interception measurements. As many as 52 tree species (including six unknown but different species) were identified in total; 27–29 tree species were present per plot (Table 1). Dominant regrowth species included *Leucosyke capitellata* (Poir) Wedd., *Leea aculeata* Blume ex Spreng., *Macaranga bicolor* Muell. Arg., and *Cananga odorata* Lamk. Hook f. & Thoms. The natural logarithm of species richness, Shannon's diversity index and species evenness (Mulder et al., 2004) for the three forest plots combined were 3.9, 3.2 and 0.8, respectively, suggesting tree species were present in rather similar numbers. Forest floor cover by leaf litter in the middle plot (measured once a month on one 1-m^2 parcel in each of 12 sub-plots of 5 m × 5 m between January and June 2014) was 51% on average (range 15–78% amongst the 12 sub-plots), while herbs and seedlings represented 12% cover on average (range 4–33%).

3. Methods

3.1. Field measurements

3.1.1. Determination of rainfall interception

Rainfall interception loss (I in mm/collection) was determined as the difference between gross rainfall (P in mm/collection) and net precipitation (i.e. throughfall TF + stemflow SF, both in mm/collection) over the one-year study period (1 June 2013–31 May 2014). Gross rainfall was measured in an agricultural patch just east of the Manobo forest at an elevation of 40 m a.s.l., as well as on the upper ridge of the study catchment at 220 m a.s.l. using a tipping-bucket rain gauge (RG3, Onset Computer Corporation, USA) connected to a HOBO Pendant event data-logger. The resolution of the rainfall recorders was 0.25 mm per tip (confirmed by manual calibration). Single tips (making up 0.85% of the annual total) were not included in the evaluation of rainfall characteristics because of the unknown duration of rainfall they represented. Events were separated by a rainless period of at least 4 h to allow full drying of the canopy (Schellekens et al., 1999; Dietz et al., 2006). The orifices of the two recording rain gauges were placed at ~1 m above ground-level to avoid ground-splash effects. Generally, the average of the amount recorded by the upper and lower tipping-bucket gauges was used as the rainfall input for the interception measurement plot, which was situated at an intermediate elevation of 110 m a.s.l. Occasional gaps in the record of either gauge were filled using corresponding data for the other recording gauge as the respective rainfall amounts were strongly correlated. (P_{upper} = 0.91 P_{lower}; r^2 = 0.975). No correction was made for wind speeds (which were generally low: 1.9 m s^{-1} on average at Tacloban Airport and 1.7 m s^{-1} at an exposed hilltop in the nearby (3.5 km) Basper grassland catchment), not even during typhoon Haiyan, because potential corrections at such extreme wind speeds would lead to very high, but unverifiable, rainfall inputs (cf. Førland et al., 1996). Instead, it was assumed that the amount of rainfall measured at a relatively sheltered valley-bottom site in the Basper grassland during typhoon Haiyan was representative for the rainfall at the study forest. In addition, the catch of a recording cylindrical fog gauge located next to the anemometer at the Basper hilltop and having a 100% catch efficiency for near-horizontal wind-driven rain (Frumau et al., 2011) was used to estimate the extra inputs of wind-driven rain during the Haiyan event. Because this type of passive fog gauge has a higher catch efficiency than does a live vegetation canopy (Bruijnzeel et al., 2005), the resulting catch must be considered to represent a maximum value. A standard manual rain gauge (100 cm^2 orifice) was placed next to the lower recording gauge as a check. Event rainfall totals for each gauge type did not differ significantly and were strongly correlated (P_{lower} = 1.01$P_{standard}$; r^2 = 0.98). In addition, a manual collector of the same type as used for the TF measurements (see below for description) was placed next to the lower recording gauge. Again, measurements for the two types of gauges were strongly correlated (Y = 1.05X, where Y = manual gauge and X = recording gauge; r^2 = 0.99). Before typhoon Haiyan, the manual rainfall- and TF gauges were generally emptied after each significant event (i.e. on the same day or the next). However, after the passage of typhoon Haiyan on 8 November 2013, the trail to access the interception measurement site was blocked by numerous fallen trees and branches and the sampling frequency was decreased to once a week or occasionally longer until late February 2014. From early March onwards until the end of the study period, measurements were typically taken every five days. The continuous records of P and TF (gutters) were used to identify single storms during such intervals.

Throughfall (TF) was measured in the 10 m × 60 m mid-elevation plot (cf. Supplementary Fig. 1c). One TF gauge was assigned to each of 24 (i.e. two parallel rows of 12) sub-plots (5 m × 5 m each) and moved to a new random location within the sub-plot after being emptied for optimal sampling of so-called drip points (where TF tends to concentrate as a result of tree architecture; Lloyd and de Marques-Filho, 1988; Holwerda et al., 2006). Each TF gauge consisted of an 18-litre collector with a 25 cm diameter funnel. A metal wire mesh (1 cm × 1 cm grid) was placed inside the funnel to minimize coarse organic debris entering the sample, whereas a ping pong ball was placed in the centre of the funnel to minimize evaporative losses. The collectors were stabilized by placing them inside a metal holder equipped with pins that were pushed into the soil. Measured TF volumes were converted to equivalent water depth (in mm) by dividing the volume of water in each gauge by the funnel area (491 cm^2). Next, the regression equation linking the catch of the manual TF-type gauge

placed in the clearing next to the lower recording rain gauge was used to correct the amounts of TF collected by the funnel-type gauges. In addition, TF was measured continuously using two fixed V-shaped stainless steel gutters (200 cm × 30 cm × 15 cm each). The gutters were placed at ca. 1 m above the forest floor to avoid splash-in from the ground and at an angle of 10° to the horizontal to encourage rapid drainage. Losses by splash from the gutter system were minimized by the V-shaped nature of the sides of the gutter. Each gutter was equipped with a tipping bucket (50 ml per tip, confirmed by manual calibration up to intensities of ~2.5 mm min^{-1}) plus a data-logger (HOBO pendant event logger, Onset Computer Corporation, USA). The drainage slot at the end of each gutter was covered by a metal mesh to minimize entry of organic debris. The collecting surface of the gutters was cleaned regularly. TF volumes measured by the gutters were similarly converted to equivalent water depths (in mm) by dividing water volumes by gutter area (corrected for gutter inclination). The catch of the two gutters was strongly correlated, both before (r^2 = 0.76) and especially after typhoon passage (r^2 = 0.96–1.00 depending on the period considered) and the respective equations were used for occasional gap-filling. Finally, the amounts of TF collected by the recording gutters and the funnel-type gauges were averaged using a weighting procedure that took the relative surface areas of the two types of gauges into account (cf. Ghimire et al., 2017).

Stemflow (SF) was measured for 12 trees which were selected on the basis of three DBH categories (four trees per category): small (DBH: 5–10 cm), intermediate (DBH: 10–20 cm), and large (DBH > 20 cm). Each tree was equipped with a 25-mm (small trees) or 64-mm (large and intermediate trees) diameter plastic hose slit open along its length and fastened tightly in a spiral fashion around the tree trunk using nails and silicon sealant. Each collar ended in a 22-litre container. Stemflow volumes were measured at the same time as TF. To scale up to the plot level, SF was converted to unit ground area (mm) for a given tree category by dividing the total volume (in litres) generated by all trees of that diameter class present within the plot, by the plot area (520 m^2, corrected for slope inclination). Total SF generated by all trees (DBH > 5 cm) within the plot was derived as:

$$SF = (SF_{small} \times a + SF_{medium} \times b + SF_{large} \times c)/A \quad (1)$$

where SF_{small}, SF_{medium} and SF_{large} are the average volumes of stemflow for the respective tree size classes per event (in litres); A is the plot area (m^2) corrected for the average ground slope of 30°; and a, b, and c denote the number of small, medium, and large trees present in the interception measurement plot (51, 19 and 12, respectively). It is recognized that the amounts of SF obtained with Eq. (1) may represent an under-estimate because stemflow was not measured on trees and saplings with a DBH < 5 cm. Although SF-volumes associated with these small trees and saplings are generally small on a per-tree basis, their contribution to overall plot-scale SF can be significant in forests where they occur in large numbers (Manfroi et al., 2004; González-Martínez et al., 2017). The density of trees and saplings with DBH < 5 cm at Manobo was not quantified. Hence, the possible degree of under-estimation of plot-scale SF by the exclusion of contributions by very small trees cannot be determined, although the overall absolute effect is likely to be limited.

3.1.2. Leaf area index

To explore how changes in canopy density might affect rainfall interception loss (cf. Fleischbein et al., 2005), LAI was measured during overcast conditions on 12 occasions between early June and late October 2013 (at intervals of 1–3 weeks) at 24 positions within the middle 600 m^2 interception study plot using a CID Bio-Science CI-110 Plant Canopy Imager (cf. Supplementary Fig. 1d). No corrections were applied to account for the effect of the measurements being conducted on a fairly steep slope as the main focus was placed on relative differences in LAI and the associated over-estimation was expected to be systematic and more or less constant (Lin et al., 2011). Due to the difficulty of access associated with the infrastructural havoc brought about by typhoon Haiyan in the Tacloban area in November 2013 plus instrumental difficulties after March 2014, post-typhoon measurements were less frequent and less regular (six observations between late November 2013 and early March 2014). It should be noted that the 24 LAI sampling positions differed somewhat between successive dates because they coincided with the positions of the TF gauges which were moved regularly for optimum sampling of spatial variability. Although the temporal changes in LAI obtained in this way will include a spatial effect, this is considered to be very minor: on three occasions LAI was measured at 48 rather than 24 points and the difference between average values for the two groups of 24 data points was insignificant. Further, in an attempt to compensate the lack of field measurements between early March and mid-June 2014, a relationship was derived between the previously measured LAI-values and corresponding values provided by TERRA/MODIS satellite imagery (Knyazikhin et al., 1999) to obtain approximate monthly changes in LAI during April–June 2014 ($Y = 0.61X + 2.53$, where Y = measured LAI and X = satellite-derived LAI; r^2 = 0.58, n = 13).

3.1.3. Pre- and post-disturbance forest inventories

Two tree inventories were made on the three plots (see study site description): the first one in May 2013 (pre-disturbance situation, cf. Table 1) and the second in January 2014 (post-typhoon damage assessment). The three plots were divided into 5 m × 5 m sub-plots (n = 74) in which the position and species of all individual trees (DBH ≥ 5 cm) were determined, as well as their height (clinometer) and projected crown area (determined from perpendicular measurements of crown width and length). No measurements of crown projected area were made during the post-disturbance inventory, as many trees had lost at least part of their leaves. Instead, four categories of leaf loss were distinguished: (i) less than 25% lost, (ii) 25–50% lost, (iii) 50–75% lost, and (iv) 75–100% lost. A fifth category concerned trees whose entire crown had broken off. In such cases, the height at which the stem was broken (as measured from the base of the stem) was recorded, as well as the distance from the point of breakage to the first major branch. Further, the condition of the leaves was noted (e.g. shredded). The proportion of twig loss was assessed using the same categories as for leaf loss. The extent of crown damage was estimated further by observing the size and position of the branches that were left on the stem and the diameter of the stem at the point of breakage. Finally, a note was made whether a tree was uprooted or not. The degree of damage was also recorded for the trees that were used for the measurement of SF. Although none of these trees were uprooted during the typhoon (hence the number of sampled trees remained constant throughout the study period), three of the trees suffered serious damage (crown pruning, stem breakage; cf. Supplementary Table 3).

3.2. Modelling rainfall interception

3.2.1. The revised analytical interception model

Because the manual TF gauges overflowed during several large events and were mostly blown over during the passage of typhoon Haiyan, the revised version of the analytical model of rainfall interception (Gash et al., 1995) was used to model the total interception losses for three periods with contrasting canopy conditions, i.e. (i) 1 June–7 November 2013 (undisturbed); (ii) damaged canopy (8 November 2013–28 February 2014; and (iii) 1 March–31 May 2014 (successively recovering foliage). While an adaptation of the analytical model that takes seasonal changes in vegetation LAI into account is available (Van Dijk and Bruijnzeel, 2001), this could not be used because of a lack of LAI data for the third period (see Section 3.1.2). The revised analytical model assumes that rainfall occurs as a series of discrete events (defined here as being separated by at least 4 h without rain to allow complete drying of the canopy before the next event (see Section 3.1.1). Each event of sufficient magnitude to fully wet the

canopy is sub-divided into three phases: (i) a wetting-up phase during which P is less than the amount required to fully saturate the canopy ($P_g^{'}$); (ii) a saturated phase, during which rainfall intensity (R) exceeds the evaporation rate from the wet canopy (E); and (iii) a drying phase after all drip from the canopy has ceased (Gash et al., 1995). The amount of water needed to completely saturate the canopy is given by:

$$P_g' = -\bar{R}/\bar{E}_c S_c In\left(1 - \bar{E}_c/\bar{R}\right) \quad (2)$$

where $\bar{R}$ denotes the average rainfall intensity falling onto a saturated canopy (mm h^{-1}). Saturated canopy conditions are generally assumed to occur whenever hourly rainfall exceeds 0.5 mm (Gash, 1979; Schellekens et al., 1999). S_c is the canopy capacity per unit area of cover (mm) and is obtained by dividing the canopy saturation value (S) by the (dimensionless) canopy cover fraction (c). Similarly, the wet-canopy evaporation rate per unit area of canopy cover ($\bar{E}_c$) is derived by dividing the evaporation rate per unit area of ground $\bar{E}$ by c (Gash et al., 1995). The direct throughfall coefficient (p) is defined as the proportion of rain that reaches the forest floor directly without hitting the canopy, hence $c = (1 - p)$. Finally, evaporation from tree trunks is specified in terms of trunk storage capacity, S_t, and the proportion of rain diverted to stemflow, p_t. Gash (1979) has shown that the slope of a regression equation between observed interception loss and rainfall (on an event basis) equals $\bar{E}/\bar{R}$, if it is assumed that both $\bar{E}$ and $\bar{R}$ are constant for all storms. In this way, $\bar{E}$ (and thus $\bar{E}_c$) may be approximated from $\bar{R}$ when above-canopy climatic observations are lacking (Bruijnzeel and Wiersum, 1987; Dykes, 1997; Holwerda et al., 2012). Table 2 summarizes the respective equations used in the revised analytical model to calculate the overall interception loss.

3.2.2. Derivation of canopy parameters used in the revised analytical model

Values of p and S for the respective periods with contrasting canopy conditions were estimated using the method of Jackson (1975). In this approach, the canopy gap fraction p is derived as the slope of the regression equation linking P and TF for storms that are too small to fill the canopy storage (conventionally using events with $P \leq 1.0$ mm only). Further, to obtain the canopy saturation value, a line of unit slope is drawn through the highest data points in a graph of event-based P versus corresponding net precipitation (P_{net}) beyond an inflection point that is defined by the intersection of the two regression lines between P and P_{net} for storms that do, and those that do not, fill the canopy storage (Jackson, 1975). Rainfall at the inflection point equals ($P_{net} + S$) if evaporation losses during canopy wetting are ignored. However, drawing a line of unit slope through the higher data points to represent events with minimal evaporation losses introduces a certain measure of subjectivity for which this type of approach has been criticized (Klaassen et al., 1998). Also, neglecting evaporative losses during canopy wetting causes S to be over-estimated somewhat by the Jackson method. Therefore, Klaassen et al. (1998) advocated the use of the 'mean method' in which S is determined as the positive intercept with the Y-axis of a regression between event-based rainfall and interception loss. The stemflow parameters S_t and p_t were derived following Gash and Morton (1978) as the negative intercept and the slope of the linear regression of SF on P, respectively.

Table 2
The equations describing the five components of rainfall interception in the revised analytical model (after Gash et al., 1995). See text for explanation.

Component of interception loss	Formula
m small storms insufficient to saturate the canopy ($P < P_g^{'}$)	$c\sum_{j=1}^{m} P_j$
Wetting up the canopy in n large storms ($P_g^{'} \geq P$)	$ncP^{'} - ncS_c$
Evaporation from the saturated canopy until throughfall ceases	$\left(c\frac{\bar{E}_c}{\bar{R}}\right)\sum_{j=1}^{n}(P_j - P_g^{'})$
Evaporation after throughfall has ceased	ncS_c
Evaporation from trunks; q storms with $P > S_t/p_t$, which saturate the canopy	$qS_t + p_t\sum_{j=1}^{n-q} P_j$

Table 3
Damage to the Manobo forest inflicted by typhoon Haiyan: general assessment of the three forest plots.

Plot/Damage type	Uprooted	Crown lost	Upper portion cut	Top pruned	Canopy damaged
Lower plot					
Trees affected	0	0	12	2	96
Idem (% of total)	0	0	12	2	100
Middle plot					
Trees affected	1	1	7	9	82
Idem (% of total)	1.2	1.2	8.5	11	100
Upper plot					
Trees affected	13	2	15	41	148
Idem (% of total)	9	1.4	10	28	100

3.3. Statistical analysis

Because of the partial defoliation of the Manobo reforest during the passage of typhoon Haiyan and the subsequent gradual re-foliation of the canopy – both of which were hypothesized to have a substantial effect on the forest's capacity to intercept and re-evaporate rainfall – the one-year study period was divided into three periods representing these contrasting canopy conditions: (i) Period 1 – fully foliated prior to typhoon Haiyan (1 June–7 November 2013); (ii) Period 2 – heavily defoliated post-Haiyan (8 November 2013–28 February 2014); and (iii) Period 3 – successively recovering foliage (1 March–31 May 2014).

The rainfall, throughfall and stemflow data were not normally distributed. Therefore, the Kruskal-Wallis test was used to test for differences between median values for the different periods followed by the Mann-Whitney-Wilcoxon test for pairwise comparisons between groups after applying a Bonferoni correction. A significance value of p = 0.05 was used throughout. Statgraphic Centurion XVII version 17.2.00 software was used for all statistical analyses.

4. Results

4.1. Effect of typhoon Haiyan on forest structure and LAI (interception plot)

Damage inflicted to the trees of the Manobo forest by typhoon Haiyan was substantial (Tables 3 and 4). Not one of the 82 trees with DBH ≥ 5 cm in the interception measurement plot (600 m^2) was left undamaged. Eighteen trees (22%) were heavily affected: two trees were uprooted, seven trees had the upper portion of their crown blown-off and nine trees had their top pruned (Table 3). All trees in the plot experienced some degree of canopy damage; 72% of the trees had at least 50% damage while 11% lost their entire crown (Table 4). Damage to the upper plot was even more pronounced due to its more exposed location (80% of the trees sustained damage level 3 or higher (i.e. > 50% leaf loss), while 28% had their tops pruned and 9% were uprooted; Table 3 and Supplementary Fig. 1a, b). The more sheltered lower plot experienced somewhat less damage (58% of trees with damage level 3 or more; Table 4).

Pre-Haiyan LAI-values varied mostly between 4.0 and 5.9 (average LAI = 5.1 ± 0.65 (SD), n = 12), with the lowest values recorded in the second half of July and late October after several weeks of relatively low rainfall (Fig. 1a). In line with the strong defoliation caused by typhoon Haiyan, LAI measured four weeks after the typhoon on 5 December 2013 was distinctly lower (2.9 ± 0.9). However, LAI recovered to 4.2–4.5 by late January 2014 (i.e. after ca. 10 weeks) and to 5.4 by early March despite low rainfall in February (Fig. 1a). The latter value is similar to the LAI at the start of the observations in June 2013 during times of ample rainfall, suggesting more or less full recovery of leaf area

Table 4
Distribution of typhoon-inflicted damage levels for individual tree crowns in the three survey plots. Percentage values in brackets are rounded off to the nearest integer.

	Lower plot		Middle plot		Upper plot	
	Trees with canopy damage	Leaf/twig loss	Trees with canopy damage	Leaf/twig loss	Trees with canopy damage	Leaf/twig loss
Damage level 1 (0–25%)	1 (1%)	1 (1%)	1 (1%)	3 (4%)	6 (4%)	6 (4%)
Damage level 2 (25–50%)	40 (42%)	39 (41%)	14 (17%)	24 (29%)	23 (16%)	23 (16%)
Damage level 3 (50–75%)	37 (39%)	38 (40%)	45 (55%)	42 (51%)	50 (34%)	50 (34%)
Damage level 4 (75–100%)	12 (13%)	12 (13%)	13 (16%)	5 (6%)	39 (26%)	39 (26%)
Damage level 5 (crown cut)	6 (6%)	6 (6%)	9 (11%)	8 (10%)	30 (20%)	30 (20%)

in the middle forest plot after about four months. The average LAI (4.0 ± 0.6; $n = 5$) for the initial post-disturbance period (8 November 2013–28 February 2014) was significantly lower than the average pre-storm LAI ($p < 0.005$). At 4.7 ± 0.5 ($n = 5$; Fig. 1a), average LAI for the period of largely recovered leaf surface area (period 3) as inferred from remotely sensed values (March–June 2014) was lower but did not differ significantly from the measured or remotely-sensed pre-disturbance averages at the 95% confidence interval.

4.2. Spatio-temporal contrasts in LAI

The temporal variation in LAI differed between sub-plots within the middle forest plot (Fig. 1b). Eighteen out of all 24 sub-plots were substantially affected by the typhoon; four weeks after typhoon passage, their LAI was more than 33% lower than the respective pre-storm averages (shaded sub-plots in Fig. 1b). The pattern of LAI recovery suggested a certain spatial clustering: LAI for some sub-plots largely recovered to the pre-storm value by late January 2014 (e.g. sub-plots 11–15, 18–21), while others took until early March (sub-plots 1–10). In

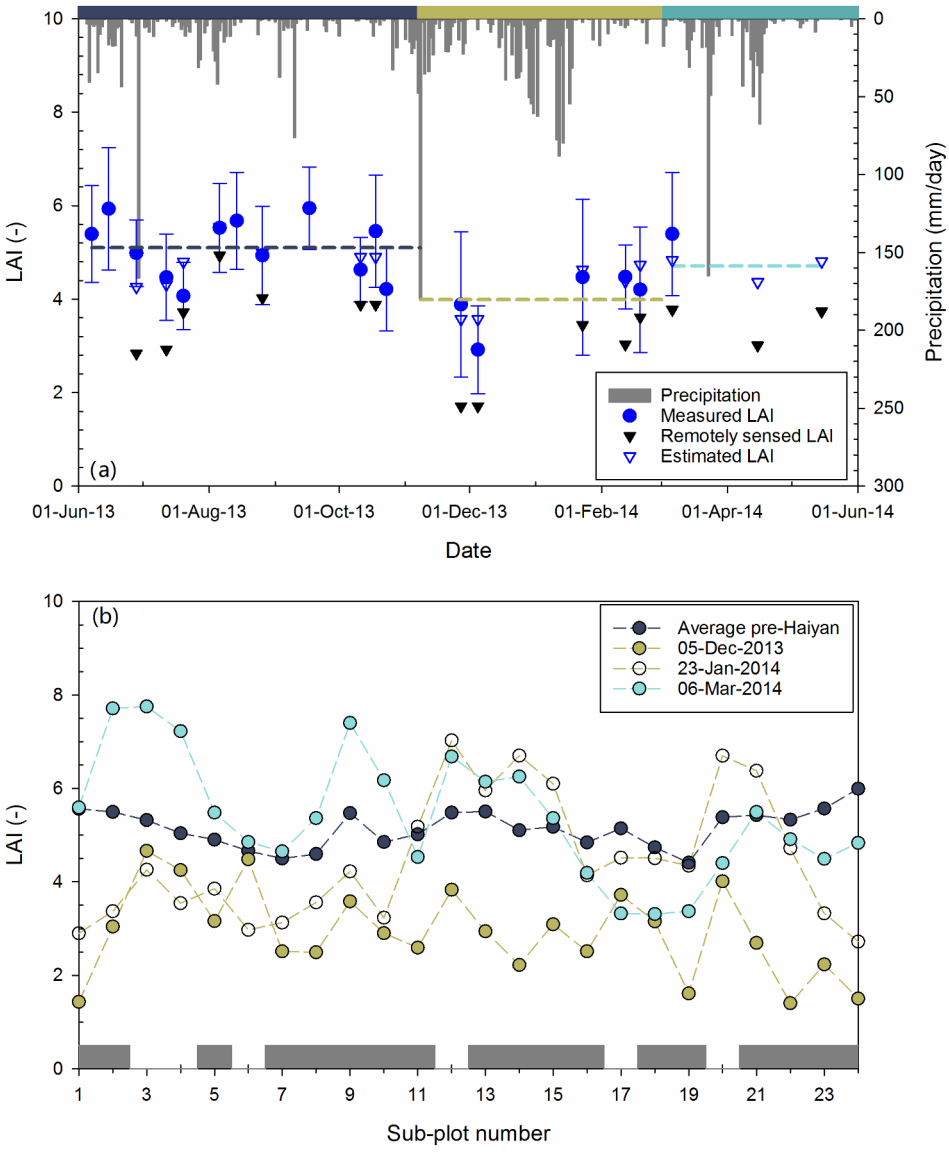

Fig. 1. (a) Average leaf area index (LAI, solid circles) plus standard deviation (error bars) based on 24 point measurements in the middle interception measurement plot at Manobo at different times during the study year. Also shown are daily rainfall, remotely sensed monthly LAI values (solid triangles) and derived LAI estimates (open triangles) assuming the relation between measured and remotely sensed LAI remained constant throughout the study period. See Section 3.1.2 for explanation; (b) LAI for sub-plots 1–24 at different points in time; sub-plots that experienced > 33% drop in LAI after canopy disturbance are indicated by shading. Note that LAI was not measured at exactly the same location in each sub-plot (see text).

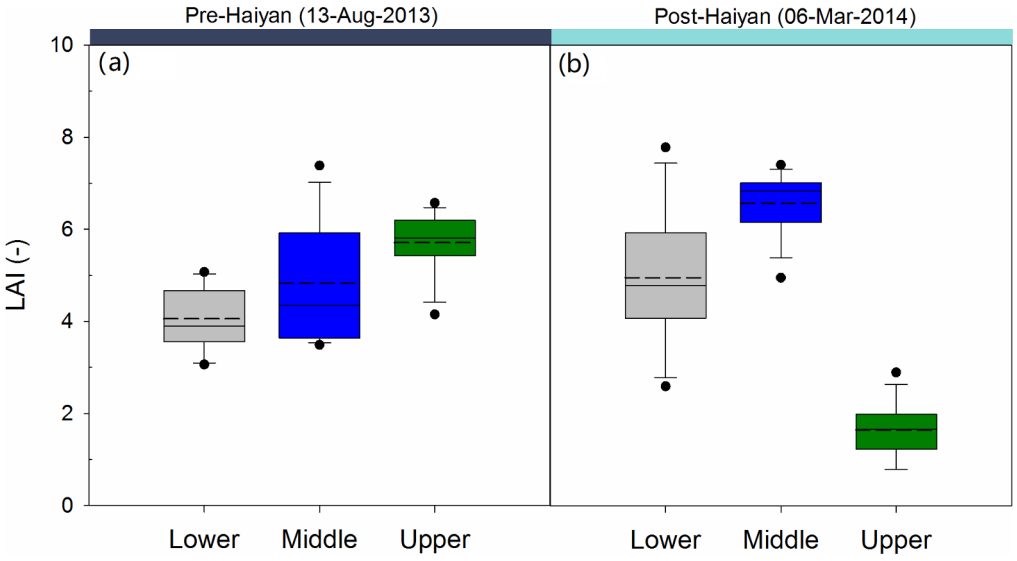

Fig. 2. (a) Box plots of LAI-values measured at 13 fixed points along the longitudinal central line of the lower, middle and upper tree inventory plots at Manobo prior to disturbance by typhoon Haiyan (13 August 2013). Average values indicated by central broken line and median values by central solid line in each box. (b) Idem on 6 March 2014 (i.e. four months after forest disturbance).

some clusters (e.g. sub-plots 2–4, 7–10, 12–14), LAI-values during the third period exceeded pre-typhoon averages, while the reverse was seen in other sub-plots (e.g. nos. 16–20; 22–24). Similarly, values determined in early March 2014 were lower than those in late January in roughly half of the sub-plots (nos. 15–24; Fig. 1b), possibly reflecting the low rainfall in February (cf. Fig. 1a). Recovery of LAI in the lowermost plot was comparable to that in the throughfall measurement site by early March 2014 (i.e. about four months after Haiyan), but that in the more heavily damaged upper plot was still very limited (Fig. 2b), despite the fact that the latter had higher LAI values than the other two plots prior to disturbance (Fig. 2a).

4.3. Rainfall characteristics

Total rainfall during the 1 June 2013–31 May 2014 study period was 3337 mm, including an estimated maximum wind-driven input of 50 mm during passage of typhoon Haiyan. Rainfall totals for the three different periods with contrasting canopy conditions were 1113 mm, 1474 mm (including the cited wind-driven rainfall) and 750 mm for the pre-disturbance, disturbed, and recovery periods, respectively. October 2013 and February and May 2014 were drier than usual, whereas June and November 2013 as well as January, March and especially April 2014 were wetter than normal (Fig. 3b). Overall, the study year was about 25% wetter than normal. The rainfall was delivered in 238 individual events (separated by $\geq$4 h without rain) that occurred on 194 days with a recorded rainfall $\geq$0.5 mm each. On 106 occasions (some of which occurred on the same day as larger events), rainfall was $<$ 0.5 mm (totaling 25 mm). Median rainfall sizes per event in the respective periods were 4.8, 5.9, and 2.8 mm.

About 57% of all events (range: 49–71%, depending on the period under consideration) occurred mostly during the day-time (between 06:00 h and 18:00 h), 37% (range: 22–45%) occurred during the night (between 18:00 h and 06:00 h), while the remaining 6–7% represented continuous rain throughout the day and night (Table 5). Events were mostly relatively small with 46–60% delivering $\leq$5 mm and 84–91% having $\leq$30 mm depending on the period under consideration. Only 2–7.5% and 1–2.5% of events were larger than 50 mm and 100 mm, respectively, with the largest falls recorded during the wet months following typhoon Haiyan (period 2; Table 5). Apart from the 8 November typhoon (203 mm plus an estimated maximum of 50 mm of wind-driven rain), each of the three periods included one large event, all related to the passage of a tropical storm, viz. 28–29 June 2013 (172 mm), 10–13 January 2014 (190 mm), and 22–24 March 2014 (220 mm). Together, these four large events delivered (at least) 785 mm of rain or 24% of the annual total (835 mm and 25% after including the estimated contribution of wind-driven rain). More than half (54–69%) of the rainfall events lasted less than 1 h, while 4–13% had a duration longer than 5 h, with the greatest occurrence of long-duration storms observed during period 2. Rainfall intensities were relatively low with as much as 46–57% of events having an intensity of 1–5 mm h^{-1} and only 1.7–5% having average intensities $>$ 20 mm h^{-1}. The absolute maximum 5-min rainfall intensity was 131 mm h^{-1}. Overall event-based average rainfall intensities for the three periods considered ranged from 6.2 to 7.7 mm h^{-1}, while due to the strongly skewed distribution the median rainfall intensities were 4.5–5.4 mm h^{-1} (Table 5).

4.4. Throughfall, stemflow, and interception losses before and after forest disturbance

Data for 68 complete manual TF- and SF-collections (i.e. no overflowing or fallen-over gauges) were selected to assess spatial variability during each of the three periods with contrasting canopy conditions (Table 6). Differences in average (and median) TF/*P* fractions between periods were small and not significant despite the fact that the coefficients of variation (CV, defined as the standard deviation divided by the mean $\times$ 100%) for the corresponding cumulative TF totals were quite modest at 12–21% (Table 6; Supplementary Fig. 2). After incorporating the gutter-based TF observations for the selected storms the differences became more pronounced between the three groups of data with overall average cumulative TF/*P*-fractions of 78%, 85% and 80%, respectively, suggesting a 7% rise in TF/*P* after defoliation (cf. Table 8 below). The stemflow data were also highly skewed and exhibited large CV-values (61–69%), but stemflow fractions (SF/*P*) were small throughout. The ratio of cumulative SF to cumulative *P* for the selected collections decreased slightly after canopy disturbance and defoliation (from 2.4% in period 1 to 2.1% in period 2; difference not significant) and was even lower after foliar recovery (1.6% in period 3; Table 6). Inserting event rainfall amounts into the relationships linking event SF to *P* for the respective periods (Fig. 7a below) gave average SF/*P* ratios of 2.7, 1.3 and 2.0% for pre-Haiyan, disturbed, and recovered conditions, respectively, with an overall annual value of 1.9%.

(Median) event-based SF/*P* ratios decreased with tree size (DBH) in an exponential fashion but differences between the relationships for the three periods were not significant (Fig. 4). Small trees (5–10 cm DBH and making up 62% of all trees with a DBH $\geq$ 5 cm within the measurement plot) were estimated to contribute 54% of the total SF at the plot scale before canopy disturbance (based on 55 collections) versus

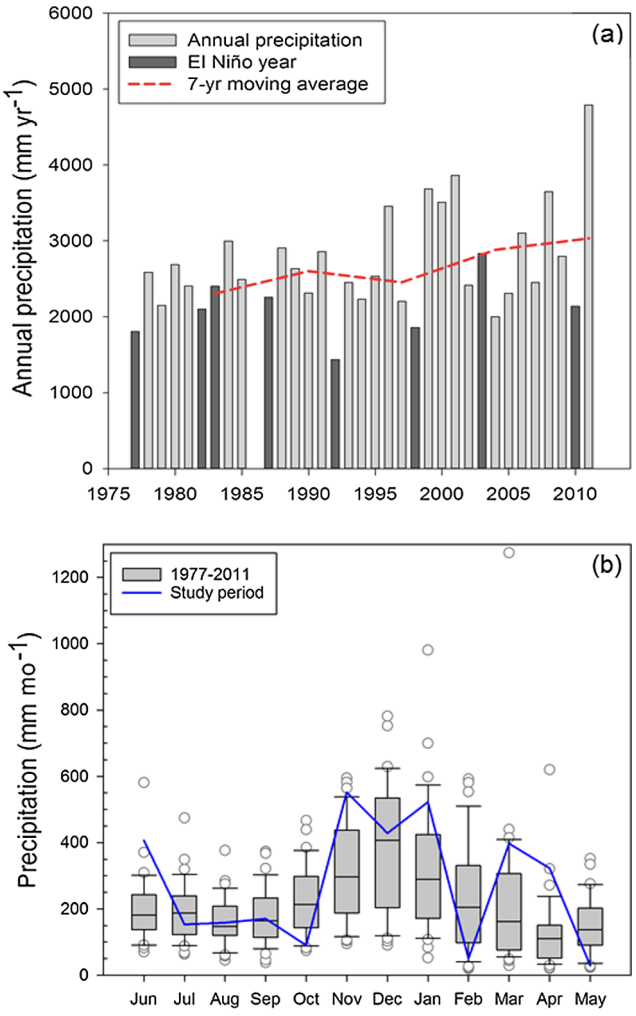

Fig. 3. Long-term rainfall at Tacloban Airport (1977–2011): (a) Individual (bars) and moving seven-year averages (line) of annual rainfall; dark bars indicate El Niño years with low rainfall; (b) Box plots of long-term monthly rainfall at Tacloban Airport along with monthly totals at Manobo during the study year (1 June 2013–31 May 2014, blue line). The central mark in the box plots represents the median value; the box edges the 25th and 75th percentiles; the whiskers extend to the 10th- and 90th percentiles. Outliers are indicated by circles. Source of data for Tacloban Airport: PAGASA Office, Tacloban. (For interpretation of the references to colour in this figure legend, the reader is referred to the web version of this article.)

63% in period 2 (19 collections). Corresponding values for large trees (DBH > 20 cm, 15% of all trees) were 14% and 11% (period 2), respectively, and 32% and 26% for medium-sized trees (DBH 10–20 cm, 23% of all trees). Total amounts of SF (mm) produced by the small trees were significantly higher compared to those for medium or large trees ($p < 0.05$) in each of the three periods ($n = 81$ collections). Pre-disturbance median SF-volumes normalized for rainfall amount (i.e. stemflow volume ratio, SVR; Holwerda et al., 2006) for different trees ranged from 0.04 to 0.21 l mm^{-1} (Supplementary Table 1) with an overall value of 0.08 l mm^{-1}. Pre-disturbance SVR-values for individual trees of a given species were comparable (e.g. *Cananga odorata*, mahogany), but values for similarly sized trees belonging to different species differed considerably (e.g. *Artocarpus* versus *Voacanga* in Supplementary Table 1). SVR-values were generally reduced after canopy disturbance and did not fully recover to pre-disturbance values during period 3 (Supplementary Table 1). Expressed in terms of the dimensionless stemflow funneling ratio (i.e. SVR/tree basal area; Herwitz, 1986), median values ranged from 1.1 to 35, with lower values usually associated with larger trees (Supplementary Table 2 and Supplementary Fig. 3). Funneling ratios generally increased with event size up to ca. 25 mm of rain (or more in the case of small trees) after which values more or less stabilized, although variability was large. Interestingly, the relationships broke down completely after forest disturbance, or changed their mathematical form in the case of some trees experiencing major structural damage (e.g. tree L4; Supplementary Fig. 3 and Supplementary Table 3). By definition, changes in funneling ratios for a given tree between periods reflected those in SVR, i.e. they dropped after canopy defoliation and structural disturbance, and recovered to some extent during period 3 for some (but not all) trees (Supplementary Fig. 3).

Table 5
Frequency distributions (%) of selected rainfall characteristics at Manobo forest during three periods with contrasting canopy conditions. Period 1: 1 June–7 November 2013; period 2: 8 November 2013–28 February 2014; 1 March–31 May 2014.

Rainfall	Frequency	Period		
Characteristic	(%)	1	2	3
Time of occurrence	Day-time	49	50	71
	Night-time	45	44	22
	Continuous	6	6	7
Event size (mm)	0.5–5	52	46	60
	5–10	20	16	14
	10–20	14	15	14
	20–30	4	7	4
	30–50	7	7	4
	50–100	2	8	3
	> 100	1	3	1
Event duration (h)	< 0.5	33	35	53
	0.5–1	26	19	16
	1–2	24	25	17
	2–5	13	9	7
	5–10	3	7	2
	10–24	1	4	5
	> 24	0	1	0
Event intensity (mm h^{-1})	1.5–5	50	46	57
	5–10	30	32	28
	10–20	16	16	14
	20–50	3	5	2
	50–100	1	0	0
	Mean	8	7	6
	Median	5	5	5

Table 6
Variability of throughfall and stemflow totals associated with 68 TF- (24 manual collectors) and SF collections (12 collectors). NB: recording gutter data for TF not included in the computation of coefficients of variation as there were only two gutters. Coefficient of variation (CV) defined as the standard deviation (SD) divided by the mean (×100%).

Throughfall	Period 1	Period 2	Period 3	All
No. of observations (*n*)	46	14	8	68
Total rainfall, *P* (mm)	654	241	439	1335
Mean total TF ± SD (mm)	543 ± 62	203 ± 26	362 ± 77	1108 ± 121
Mean total TF/*P* (%)	83	84	82	83
Coefficient of variation of TF (%)	12	13	21	11
95% confidence interval of TF (mm)	518–568	192–214	331–393	1060-1156
Stemflow	Period 1	Period 2	Period 3	All
No. of observations (*n*)	46	14	8	68
Total rainfall, *P* (mm)	654	241	439	1335
Mean total SF ± SD (mm)	15.5 ± 9.4	5.2 ± 3.6	7.2 ± 5.0	27.8 ± 17.3
Mean total SF/*P* (%)	2.4	2.1	1.6	2.1
Coefficient of variation of SF (%)	61	69	69	62
95% confidence interval of SF (mm)	10–21	4–8	4–10	18–38

Table 7
Forest structural model parameters, average rainfall intensities onto a saturated canopy, and average wet-canopy evaporation rates at Manobo during the three periods with contrasting canopy conditions. P_g' denotes the amount of rainfall (mm) required to saturate the canopy (Eq. 2). Indicators for canopy saturation value S and its use in the computation of P_g': J = Jackson (1975) method; K = mean method of Klaassen et al. (1998).

Period	Canopy saturation value (S, mm) J/K	Direct throughfall fraction (p)	Trunk storage capacity (St, mm)	Stemflow fraction (pt)	Median rainfall rate ($\tilde{R}$, mm h-1)	$\tilde{E}/\tilde{R}$	Mean wet-canopy evaporation rate ($\bar{E}$, mm h−1)	P_g' (mm) J/K
Pre-Haiyan	0.45/0.45	0.30	0.077	0.033	5.0	0.139	0.70	0.72/0.72
Damaged canopy	0.30/0.24	0.61	0.041	0.015	5.4	0.102	0.55	0.91/0.69
Recovering canopy	0.35/0.35	0.41	0.053	0.023	4.5	0.146	0.66	0.69/0.69

Table 8
Comparison of observed and modelled total interception losses at Manobo for selected rainfall events during the three periods with contrasting canopy conditions. E_{TF} and E_{OPT} denote model runs with throughfall-based and optimized wet-canopy evaporation rates, respectively. $E_{OPT\text{-}J}$ and $E_{OPT\text{-}K}$ (period 2 only) represent model runs with optimized values of the canopy saturation value obtained with the Jackson- and the mean method, respectively. Optimizing S did not improve the fit of modeled interception losses for periods 1 and 3 either.

	Period 1		Period 2			Period 3	
	E_{TF}	E_{OPT}	E_{TF}	$E_{OPT\text{-}J}$	$E_{OPT\text{-}K}$	E_{TF}	E_{OPT}
Number of events	86		51			54	
Total gross rainfall (mm)	610		203			369	
Total throughfall (mm)	476		170			293	
Total stemflow (mm)	15		2			7	
Total measured interception loss (mm)	119		31			70	
Total modeled interception loss (mm)	121	118	31	30	31	71	70
Modeled minus measured (% relative error)	1.8	−0.8	−0.1	−2.6	−0.2	1.3	−0.1
Root Mean Squared Error (mm)	0.83	0.83	0.492	0.490	0.490	0.97	0.97

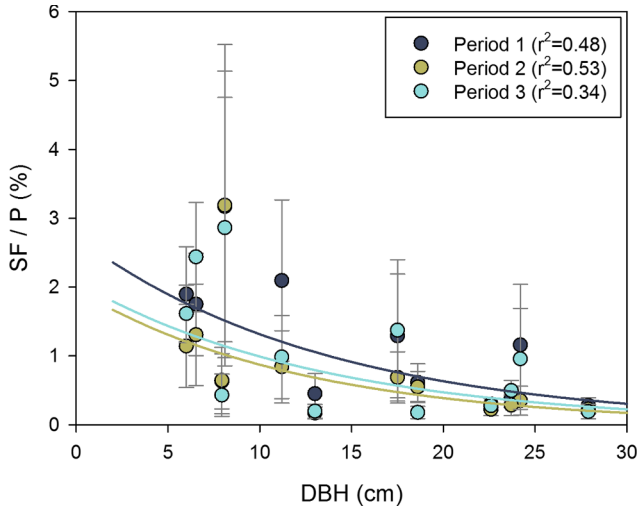

Fig. 4. Relationships between median stemflow (mm tree^{-1}, expressed as a percentage of rainfall, P) and sample tree size (represented by diameter at breast height, DBH) for the three periods with contrasting canopy conditions. Error bars represent median absolute deviation (MAD) of stemflow. Relations for the three periods were not significantly different ($p > 0.10$).

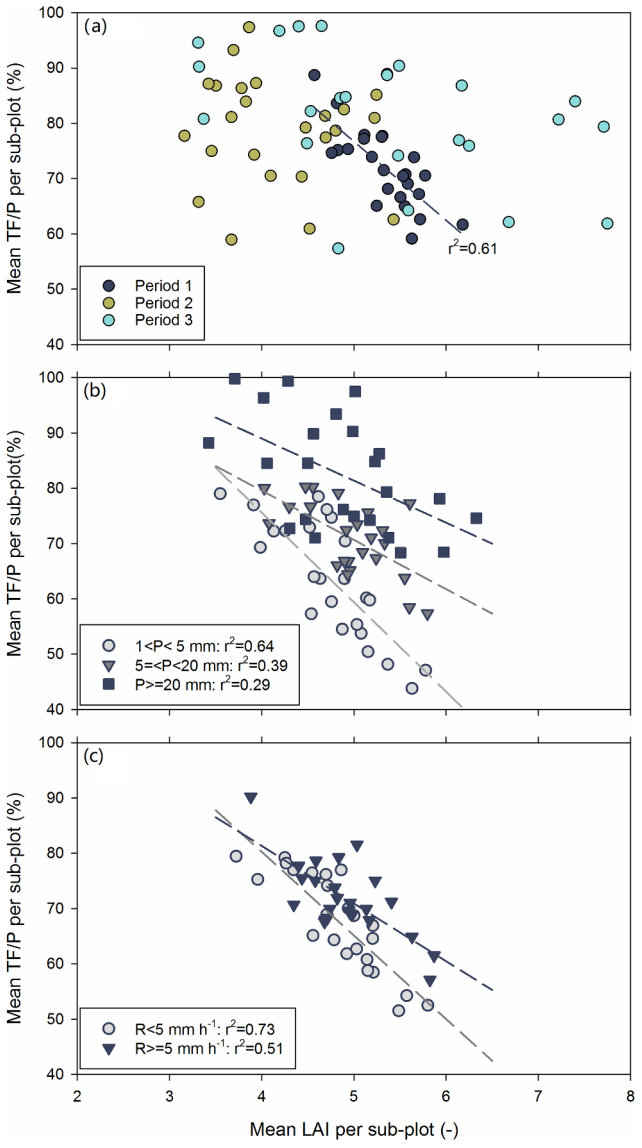

Fig. 5. (a) Relative throughfall amounts (TF/P, %) versus LAI for the 24 sub-plots in the central Manobo forest plot during three periods with contrasting canopy conditions; and mean relative throughfall prior to canopy disturbance as a function of (b) rainfall event size (P) and (c) event-averaged rainfall intensity (R).

4.5. Spatio-temporal variations in LAI and their effect on relative throughfall amounts

Average TF/P ratios for the three periods more or less mirrored the corresponding changes in LAI in an inverse manner (cf. Table 6 and Fig. 1). Similar negative trends were obtained when linking average TF/P to average LAI per period for the 24 sub-plots (Fig. 5a). The relation was steepest and strongest for the pre-disturbance period ($r^2 = 0.61$; $n = 59$ collections), poor (and much less steep) for the canopy recovery phase (period 3; $r^2 = 0.20$, $n = 17$ collections) and non-existent for the period with maximum defoliation (period 2; $r^2 = 0.02$, $n = 9$

collections). Examining pre-disturbance data only and distinguishing between three event size classes ($P < 5$ mm, 5–20 mm, and ≥20 mm) maintained the negative trends, with the strongest correlation ($r^2 = 0.64$, $n = 15$ collections) and steepest slope for the smallest category (differing significantly from the relations for the larger event classes). The slopes of the corresponding equations for the other two event categories did not differ significantly from each other but their coefficients of determination declined with increasing event size (Fig. 5b). A similar pattern was found when distinguishing between rainfall intensity classes (Fig. 5c). Thus, LAI appeared to exert the strongest influence on relative TF amounts (and hence relative I) prior to canopy disturbance for small ($P < 5$ mm) and low-intensity (1–5 mm h^{-1}) events (Fig. 5b, c).

4.6. Canopy structural parameters as derived from throughfall and stemflow measurements

Values for the main canopy parameters used in the interception modeling (canopy saturation value S, direct throughfall coefficient p, trunk storage capacity S_t and the proportion of rainfall diverted to stemflow p_t) were derived for the three periods with contrasting canopy conditions from measured P, TF and SF for selected storms (Figs. 6 and 7). Table 7 summarizes the results for the respective periods, along with the corresponding values of the amount of rainfall required to fully wet the canopy (P_g'), and average evaporation rates from a saturated canopy ($\bar{E}$) following Gash (1979).

The canopy saturation value for the Manobo forest derived with the Jackson method dropped from 0.45 mm for the pre-Haiyan period (period 1) to a low 0.30 mm during the period with the most extensive canopy damage (period 2), and recovered somewhat subsequently (0.35 mm; Fig. 6 and Table 7). Values of S derived with the 'mean method' were identical to those obtained with the Jackson method for periods 1 and 3, but slightly lower (0.24 mm) for period 2 (Figs. 6, 7b and Table 7). Changes in the direct throughfall coefficient mirrored those for S in that p increased from 0.30 for period 1 to as high as 0.61 during period 2 and 0.42 for period 3 (Fig. 6 and Table 7).

Although SF constituted only a small fraction of incident P, regardless of canopy conditions (Table 6), the regression equations linking SF and P were quite strong (Fig. 7a). Stemflow coefficients (p_t) ranged from 0.033 for period 1 to 0.015 during period 2, with an intermediate value (0.023) for period 3.

Correlations between event-based interception loss I and P were less strong than those for SF (0.82–0.95) with coefficients of determination ranging from 0.37 (period 2) to 0.69 (period 3) and 0.70 (period 1; Fig. 7b). The slopes of the respective equations (i.e. $\bar{E}/\bar{R}$; cf. Gash, 1979) varied from 0.14 (period 1), to 0.10 (period 2) and back to 0.15 (period 3), suggesting values of 0.70, 0.55 and 0.66 mm h^{-1}, respectively, for $\bar{E}$ using median rather than average rainfall intensities in view of the strong negative skewness of the latter (cf. Table 5). Finally, combining the values of S, c and $\bar{E}_c/\bar{R}$ for the respective periods gave values of ca. 0.7 mm for the amount of rainfall required to saturate the canopy (Eq. (2)) P_g' (Table 7).

4.7. Model application

To estimate period-totals of interception loss that included a number of large storms for which TF and SF data were incomplete due to overflowing or disturbed collectors, the revised analytical model of rainfall interception was tested against measured I for the data from which the forest structural and other model parameter values listed in Table 7 were derived. The model overestimated the observed total interception loss for the pre-disturbance and recovery periods only slightly (by 1.8 and 1.3%, respectively, with corresponding Root Mean Square Errors of 0.83 and 0.97 mm), while effectively equaling the observed I for period 2 (−0.1%; RMSE = 0.49 mm) (Table 8).

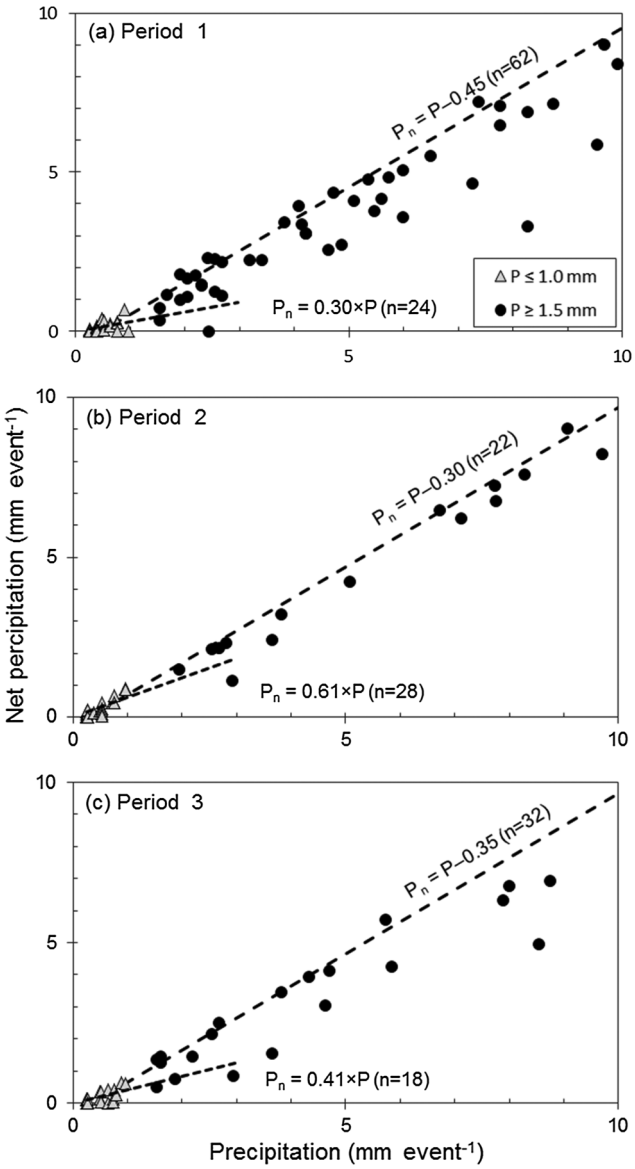

Fig. 6. Derivation of the canopy structural parameters S (canopy saturation value, in mm) and p (direct throughfall fraction) for the Manobo reforest using the Jackson method for the three periods with contrasting canopy conditions.

Optimizing the model for $\bar{E}_c/\bar{R}$ to minimize the RMSE between modeled and observed I (cf. Schellekens et al., 1999; Ghimire et al., 2017) reproduced observed interception totals for periods 1 and 3 slightly better in terms of relative model error (−0.8% and −0.1%, respectively), but did not reduce the associated RMSE-values. Optimizing the value of S did not have any effect on model performance. Optimizing wet-canopy evaporation rate and the canopy saturation value did not improve predictions for the second period either (Table 8 and Fig. 8). Next, the best-performing model parameterization was applied to estimate period- and annual totals of I using the complete rainfall record. Overall annual I estimated in this way amounted to 514 mm (15% of P) with period-values ranging from 18% prior to forest disturbance (period 1) to 12% after extensive defoliation (period 2), and 17.5% during the successive canopy recovery phase (period 3) (Table 9).

The effect of canopy disturbance by typhoon Haiyan on annual I was assessed by comparing the previously obtained periodical and annual losses (reflecting the changing canopy conditions) with that predicted by the model using pre-disturbance parameter values throughout (572 mm or 17% of annual P; Table 9). The model attributed nearly

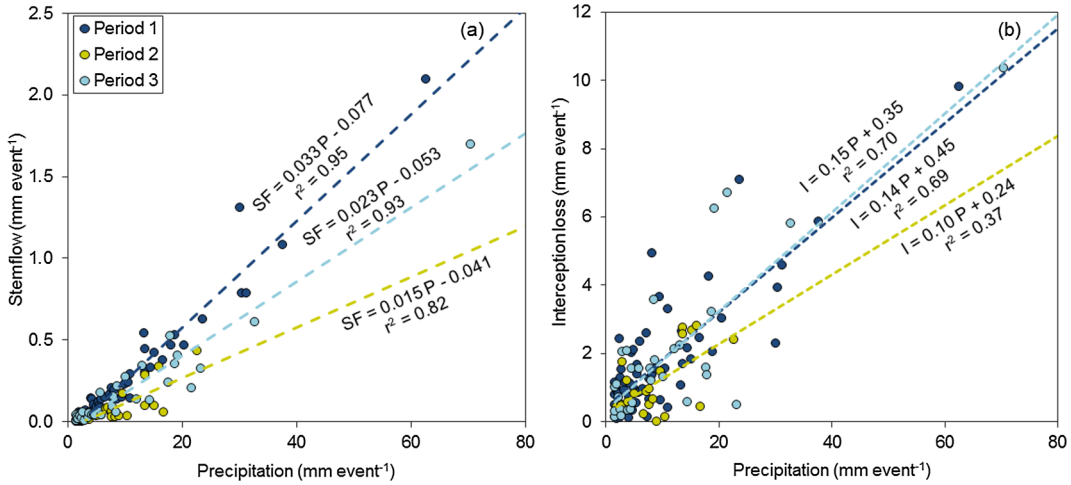

Fig. 7. Relationships between event-based gross rainfall and (a) stemflow, and (b) interception loss (all in mm per event) for the three periods with contrasting canopy conditions.

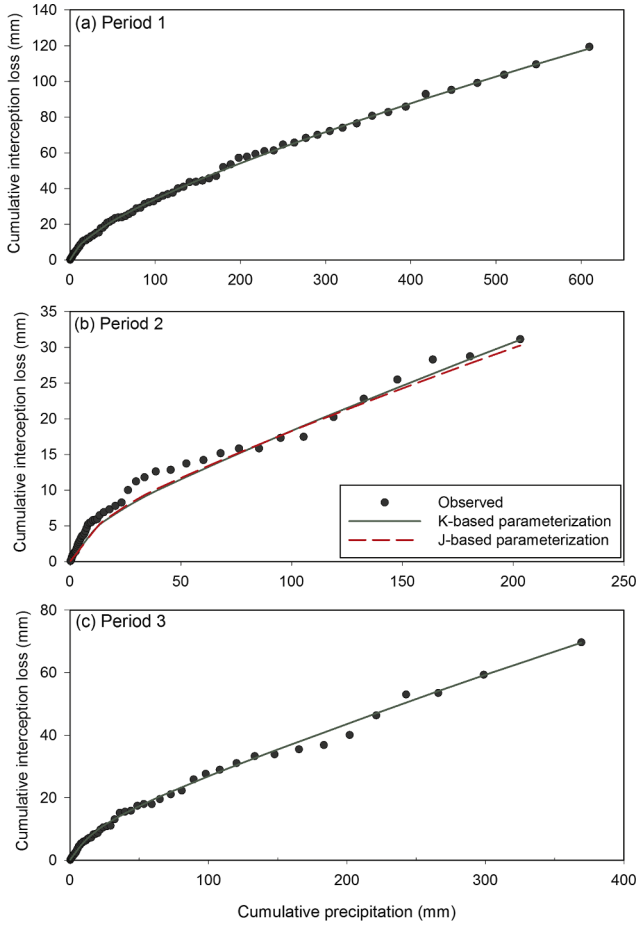

Fig. 8. Observed and modeled cumulative interception losses as a function of cumulative rainfall for selected events during the three periods with contrasting canopy conditions. The solid lines denote simulations using canopy saturation values obtained with the 'mean method' and the broken line the simulation with the canopy saturation values derived with the Jackson method (period 2 only). See Table 8 for companion information.

three-quarters (73%) of the predicted annual *I* for undisturbed canopy conditions to evaporation from a fully wetted canopy, 18% to evaporation after rainfall has ceased (drying-up phase), and 4% by evaporation during small storms. Losses associated with canopy wetting (2%) and evaporation from trunks (3%) were equally minor (Table 9). At 58 mm (i.e. 572 minus 514 mm), the inferred reduction in annual interception loss due to the temporary defoliation caused by typhoon Haiyan and the subsequent gradual recovery of LAI at the middle plot is modest at best (equaling only 1.7% of annual *P* but 10% of *I* for an undisturbed canopy).

4.8. Wet-canopy evaporation versus rainfall intensity during large storms

The data set used for the calibration of the revised analytical model did not include four very large events (during which most, if not all, manual TF collectors overflowed). To test whether wet-canopy evaporation rates were substantially different during these very large (172–220 mm) events, hourly TF amounts recorded by the two large gutters during the raining episodes of three of these events (excluding typhoon Haiyan because of its excessive winds and the disturbing effects these had on the measurement of both *P* and TF as well as the forest canopy itself) were compared with corresponding hourly rainfall totals to derive associated amounts of apparent *I* (all in mm h^{-1}). Hourly evaporative losses were positively correlated with rainfall intensity, especially for individual events (Fig. 9). Maximum values of hourly interception loss inferred in this way were as high as 5–6 mm and therefore far exceeded the period-average wet-canopy evaporation rates (0.55–0.70 mm h^{-1}, Table 7). Pertinently, the relationship was steeper for the 10 January 2014 event during which time LAI was much reduced (Figs. 9 and 1a).

5. Discussion

5.1. Typhoon effects on forest structure

Although all trees in the three sample plots (total area 1850 m^2) were affected by typhoon Haiyan (Tables 3 and 4), spatial contrasts in the level of incurred canopy damage reflected clear differences in site exposure. Damage was more extensive, and recovery of LAI much slower, in the more exposed upper forest plot compared to the more sheltered middle and lower plots (Table 4 and Fig. 2b). Winds in excess of 100–130 km h^{-1} can damage trees lethally within several hours, while wind speeds above ca. 60 km h^{-1} typically cause large-scale defoliation (Scatena et al., 2005). Maximum wind speeds recorded around the time of the cyclone's landfall in the early morning of 8 November 2013 were as high as 314 km h^{-1} (87 m s^{-1}; Rabonza et al., 2015) with wind speeds sustained over 10 min of up to 230 km h^{-1} (64 m s^{-1}; Nguyen et al., 2014). Wind speeds experienced by the trees on the ridges and uppermost slopes of the Manobo forest are likely to have

Table 9
Modeled individual components of period-total and overall annual interception losses for the Manobo reforest during the study year, plus the estimated annual interception loss for undisturbed canopy conditions using the revised analytical model of rainfall interception with canopy saturation values based on the mean method.

	Period			Annual total (mm)	
Interception component (mm)	1	2	3	Using actual parameters per period	Using pre-disturbance parameters
m small storms ($< P_g'$) insufficient to saturate canopy	9	5	4	18	23
Wetting up of the canopy; *n* storms $> P_g'$ which saturate the canopy	5	3	3	11	11
Evaporation from the saturated canopy	137	152	103	392	418
Evaporation after throughfall has ceased	44	18	19	81	104
Evaporation from stems	7	3	2	12	16
Total modelled interception loss	**202**	**181**	**131**	**514**	**572**

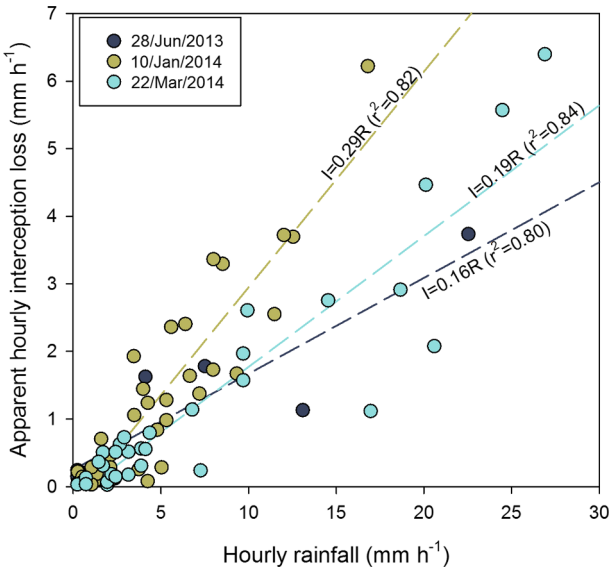

Fig. 9. Hourly apparent interception loss (*I*) versus hourly rainfall intensity (*R*) during three exceptionally large storms at Manobo before canopy disturbance (dark circles), during the period of maximum defoliation (olive circles), and after initial canopy recovery (light-blue circles). Stemflow was not included, hence interception losses are slightly over-estimated. (For interpretation of the references to colour in this figure legend, the reader is referred to the web version of this article.)

been equally high. Generally, older and therefore taller and more prominent trees tend to be more vulnerable to crown damage by high wind (Basnet et al., 1992; Lin et al., 2011), but large trees were effectively lacking at Manobo, where 85% of the trees had a DBH < 20 cm. Rather, in view of the fact that fast-growing species of low wood density are more amenable to damage than slower-growing later successional species (Putz, 1983; Zimmerman et al., 1994), the observed high spatial variability in leaf area reduction after typhoon passage (Fig. 1b) may reflect a combination of differences in individual tree height (affecting local turbulence and crown exposure) and wood strength (branch breakage). However, despite the extensive crown damage recorded during the January 2014 survey (Tables 3 and 4), LAI values for the relatively sheltered middle and lower plots reached pre-disturbance values again after ca. four months (6 March 2014, Fig. 2). Comparable spatial contrasts in forest damage as a function of site exposure have been reported for Puerto Rico (Walker, 1991; Scatena et al., 1993, 1996) and Taiwan (Lee et al., 2008). It has been suggested that planted forests (like the Manobo reforest) may be less well adapted than natural forests, and thus suffer greater typhoon/hurricane damage (e.g. Caribbean pines in Nicaragua and Fiji: Boucher et al., 1990; Waterloo, 1994; mahogany in Puerto Rico: Basnet et al., 1992). However, the greater damage to mahogany trees in the Puerto Rican case was caused in part by the fact that introduced tree species had been preferably planted in moister valley soils that provided less anchoring opportunity (Basnet et al., 1992). Similarly, typhoon damage to natural broad-leaved forest in Central Taiwan was reported to be greater than that to nearby coniferous plantations due to differences in site exposure (Lee et al., 2008). All (exotic) mahogany and *Gmelina* trees at Manobo were severely damaged by typhoon Haiyan and were subsequently felled during a timber salvaging operation. With the expected gradual increase in strength of typhoons in general (Knutson et al., 2010; Kossin et al., 2014) and an intensification of 'super-typhoons' in particular due to global warming-induced upper-oceanic freshening (Balaguru et al., 2016), the structure and development of secondary forests in the cyclone-ridden north-western tropical Pacific (de Gouvenain and Silander, 2003) is likely to be affected increasingly by typhoons in the future (see Lin et al. (2011) and Yao et al. (2015) for a discussion of the ecological consequences), despite a slight decrease in the total number of tropical storms crossing the Philippines in recent years (Cinco et al., 2016).

5.2. Forest disturbance effects on interception loss

Studies of the effects of large-scale tropical forest destruction by wind (as opposed to gap creation by selective logging: Asdak et al., 1998b; Chappell et al., 2001) on rainfall interception loss are rare. Long-term rainfall and throughfall data for the Bisley forest in Puerto Rico suggested a return to normal TF/*P* ratios within a year after forest wreckage by Hurricane Hugo (Scatena et al., 1996), while Heartsill-Scalley et al. (2007) reported further enhanced (but unquantified) TF/*P* ratios for the seven-week period after passage of Hurricanes Bertha (1996) and Georges (1998) at Bisley compared to the preceding seven-week period. Neither study attempted to separate the (strong) seasonal variation in TF/*P* for the Bisley forest (Schellekens et al., 1999) from that incurred by actual storm damage, so that the overall effect on annual interception loss remains unknown. Waterloo (1994) estimated *I* from two *Pinus caribaea* plantations in Fiji before and after they were struck by Cyclone Sina in November 1990. There was a major reduction in wet-season *I* for the younger of the two plantations (from 22% in 1990 to 11% shortly after the storm in 1991), but values for pre- and post-cyclone dry-season *I* were already similar (2% higher in 1991 after seven months of re-foliation). Pre- and post-storm differences for an older stand were less pronounced (3–4% reduction in *I*) and possibly reflected a smaller reduction in LAI (Waterloo, 1994). This reduction in interception loss is similar to the typhoon-induced change in annual *I* estimated for the Manobo reforest (−1.7% of annual *P*, Table9), although the absolute difference is larger because of the much higher rainfall in the Philippines. Neal et al. (1993) also found a 4% decrease in *I*/*P* for a mature beech forest in the southern U.K. during the first year after it was hit by a major storm. Summarizing, the effect of major canopy disturbance by high winds on rainfall interception loss appears to be both temporary (4–12 months) and comparatively modest (< 4% of annual *P*), although it remains to be seen what the cumulative effects

will be of more intensive or more frequent disturbances in future (cf. Cinco et al., 2016; Lin et al., 2011; Yao et al., 2015).

It is of interest to compare these wind-induced disturbance effects with the impact of seasonal changes in LAI on interception loss (i.e. defoliation but no added gap creation) and that of selective logging (gap creation only). Tanaka et al. (2015) did not find any difference in TF/*P* ratios for mature teak plantations in Thailand during the leafless and leafed states. Rainfall amount was the only variable explaining TF during the growing season, while temperature, maximum wind speed, and rainfall intensity were also influential during the leafless (dry) season. In a companion study on the effects of climatic and canopy conditions on SF production by teak trees, Tanaka et al. (2017) reported increased SF/*P*-ratios during the leafless state for five out of nine sampled trees, no significant change in three others, and a reduction in the one remaining sample tree. Interestingly, the trees exhibiting an increase in SF/*P* did not experience shading by neighbouring crowns in the leafed state whereas the other trees did. Despite considerable variability between individual trees, the median stemflow funneling ratio increased during the leafless season (Tanaka et al., 2017). Chen and Li (2016) did not find any difference in wet- and dry-season *I* from a sub-tropical forest in Taiwan, despite major contrasts in seasonal LAI (52% drop in the dry season). Although the TF/*P* ratio increased somewhat during the dry season, this was compensated by an equal *reduction* in SF/*P*. Pertinently, while evaporation from a wetted canopy was the dominant interception component throughout the year, the ratio between the latter and the amount contributed by the drying-up phase more than tripled (1.4 versus 4.9) in the dry season. This marked shift reflected both a lower dry-season canopy saturation value (*S*) – causing smaller losses during canopy drying – and a much lower average dry-season rainfall intensity (2.8 versus 5.8 mm h^{-1}) (Chen and Li, 2016; cf. Gash et al., 1995). At Manobo, where median rainfall intensities were effectively similar between periods (Table 5), the reduction in *S* following the passage of typhoon Haiyan from 0.45 mm to 0.24–0.30 mm (Table 7) also caused a reduction in the inferred contribution of canopy drying to total *I* (from 22% to 10%). Predicted evaporation from the saturated canopy increased from 68% prior to forest disturbance to 84% after typhoon Haiyan (Table 9), implying an upward shift in the ratio between the two interception components from 3.1 to 8.4. In agreement with the findings of Chen and Li (2016) for natural forest in Taiwan, but unlike the results obtained by Tanaka et al. (2017) for teak plantations in Thailand, stemflow at Manobo (both in terms of SF/*P* ratios and funneling ratios) decreased after defoliation by typhoon Haiyan and recuperated somewhat after the LAI increased again in period 3 (Fig. 7b and Supplementary Fig. 3). However, SF production is the result of complex interactions between both spatio-temporal variations in tree architecture and a range of climatic factors (Tanaka et al., 2017). Thus, simple comparisons between leafed and leafless states are unlikely to provide the full answer, just like predictive approaches based on tree characteristics do not get very far, especially not in species-rich tropical forests (Zimmermann et al., 2015).

One might expect gap creation during logging to increase the aerodynamic conductance (g_a) due to the associated increase in canopy surface unevenness, thereby enhancing turbulent exchange and thus evaporative losses during and immediately after rainfall. Instead, Asdak et al. (1998a) reported a marked *decrease* in g_a and *I*/*P* upon opening a rain forest canopy in Kalimantan. Similar decreases in g_a were derived by Deguchi et al. (2006) for the leafless phase of a warm-temperate deciduous forest in Japan and by Teklehaimanot et al. (1991) for a series of temperate coniferous plantations of progressively lower stocking. None of these studies provided a physical explanation for the reduction in g_a, but it is likely that defoliation and opening of the canopy by logging or thinning also leads to 'deeper' ventilation (i.e. a lowering of the displacement- and roughness lengths, d and z_0), and thus to a lower g_a (Thom, 1975). However, as stated by Asdak et al. (1998a) and indicated by our modeling (Table 9), the observed reductions in *I*/*P* after canopy opening or defoliation reflect both changes in wet-canopy evaporation rates and reduced canopy saturation values (cf. Table 7).

5.3. Effects of canopy heterogeneity on throughfall

Relative throughfall amounts (TF/*P*) in the Manobo forest were inversely related to canopy density as represented by measurements of LAI above individual TF collectors under undisturbed canopy conditions (r^2 = 0.61; Fig. 5a). Corresponding relations for the two post-typhoon periods were less steep and not significant (Fig. 5a). As such, LAI alone is a rather poor predictor of on-site TF/*P*, as also reported for mature rain forests in Ecuador (r^2 = 0.12; Fleischbein et al., 2005), Puerto Rico (r^2 = 0.12– 0.21; Holwerda, 2005), and Indonesia (r^2 = 0.02; Dietz et al., 2006) as well as for tree plantations in Panamá (Park and Cameron, 2008). In addition, results become poorer as rainfall event size or intensity increased (Fig. 5b, c), possibly because of the larger variability in event sizes involved with increasing rainfall compared to the relatively small variation in TF/*P*; cf. Holwerda, 2005). Somewhat better results were obtained when using a measure of canopy openness instead of LAI (Fleischbein et al., 2005) or using canopy 'depth' and openness as added variables (Park and Cameron, 2008; cf. Dietz et al., 2006). However, the strong dependency of such relations on rainfall amount or intensity (Fig. 5b, c) already indicates that forest structural parameters alone have limited predictive capacity in this regard. In addition, many of these structural parameters are correlated with one another, rendering the use of multiple regression approaches problematic (Zimmermann et al., 2013). In a particularly stringent study involving multiple stands of different ages and characteristics under similar climatic conditions, Zimmermann et al. (2013) concluded that the best TF/*P*-predictor was the basal area fraction contributed by small trees (r^2 = 0.72).

5.4. Interception loss from regenerating tropical forests: the Manobo reforest in perspective

Despite the modest age and stature of the Manobo reforest (23 years and 7.3 m tall at the start of the interception measurements), both the observed cumulative pre-Haiyan interception loss for selected storms (18%, Table 8) and the modeled annual *I* for undisturbed canopy conditions (17%, Table 9) are in the upper part of the range of values derived for *old-growth* lowland evergreen rain forests in South-east Asia (8–22%), as well as those for most regenerating forests (3–21%; Table 10). Although results obtained for different forests reflect differences in canopy density and local rainfall intensities, for a given forest type there appears to be a distinct trend towards lower *I*/*P*-values for studies employing a larger number of TF-collectors (e.g. old-growth lowland forests in Table 10). Such findings are usually interpreted in terms of the ability of the sampling design to adequately include 'drip points', i.e. points of locally enhanced TF/*P*-ratios (Lloyd and de Marques-Filho, 1988; Manfroi et al., 2006). Yet it would be premature to attribute the relatively high *I*/*P*-value derived for the Manobo reforest to inadequate sampling. On top of the 24 roving TF gauges, two large gutters were used, which effectively doubled the sampling area to the equivalent of 48 gauges. Also, with coefficients of variation (CV, %) for our mean (manually obtained) TF estimates ranging from 11.5% (period 1) to 21% (period 3), throughfall variability at Manobo (Table 6; cf. Supplementary Fig. 2) was (much) less than that observed for more biodiverse mature rain forests in Central Kalimantan (36% for 18 roving gauges; Vernimmen et al., 2007), Panamá (49% for 30 fixed gauges, Macinnis-Ng et al., 2012) and Puerto Rico (23% for 30 roving gauges; Holwerda et al., 2006). Rather, our cumulative CVs were comparable to the 15–24% reported for lowland rain forest after some selective logging in North-east Borneo and using a very large number of fixed TF samplers (n = 80; Chappell et al., 2001).

While the interception results for regenerating tropical forests collated in Table 10 vary widely as a result of differences in canopy

Table 10
Studies of interception loss (*I*) in regenerating tropical forests with at least six months of data collection and listed in order of vegetation age. Results for selected old-growth forests added for comparison. MAP = mean annual rainfall; TF = throughfall; SF = stemflow; H = canopy height (m); LAI = leaf area index; BA = basal area (m^2 ha^{-1}). Values rounded off to the nearest per cent of incident rainfall except for stemflow.

Location and forest type	Age (yr)	MAP (mm)	H (m)	LAI –	BA (m^2 ha^{-1})	TF (%)	SF (%)	*I* (%)	Sampling set-up
Lowland secondary forest									
Costa Rica[a]	1	4000	–	–	–	68	4	28	19 fixed, 60 mo
E. Amazonia[b]	2.5	2470	1.3	4.6	–	65	23	12	15 roving, 1 yr
E. Amazonia[c]	4	2470	2.6	4.2	–	77	16	7	50 roving, 2 yrs
	5		3.4	–	–	72	20	8	Idem
C. Amazonia[d]	3.5	2620	~5	–	–	77	20	3	6 fixed, 1 yr
Panamá, SF2 site[e]	6–10	2250	7	5.2	–	85	–	< 15	30 fixed, 16 mo
E. Amazonia[b,#]	10	2470	5	4.6	–	38	41	21	15 roving, 1 yr
Panamá, SF3 site[e]	15	2250	–	5.4	–	84	–	< 16	30 fixed, 16 mo
Leyte, Philippines[f,*,0]	23	2660	7	5.1	15	81	2	17	24 roving, 1 yr
Old–growth lowland rain forest									
E. Amazonia[g,@]		3025	–	–	25	85	0.4	15	38 fixed, 1 yr
E. Amazonia[h]		–	20	5.3	–	86	1	13	30 roving 14 mo
C. Amazonia (Ducke)[i]		2440	30	5.7	–	89	2	9	36 roving 16 mo
C. Amazonia (Ducke)[j]		2440	30	6.6	–	80	–	20	20 fixed, 13 mo
C. Amazonia (Cuieiras)[k,+]		2440	30	6.1	34	86	0.6	13	6 gutters, 1 yr
N.E. Borneo (Sabah)[l]		2800	45[m]	4.3[n]	31[m]	81	2[o]	17	30 fixed, 1 yr
N.W. Borneo (Sarawak)[p]		2740	55	–	145	85	3	12	20 fixed, 3 yrs[$]
			55	6.2	42	88	3.5	8.5	+80 roving[$$]
C. Borneo (Indonesia)[q]		3560	40	–	39	87	1.4	11	50 roving, 6 mo
C. Borneo (Indonesia)[r]		2995	40	–	29	83	1	16	18 roving, 1 yr
N. Queensland (Oliver Crk)[s,*]		3070	27	4.2	64	75	3	22	6 gutters, 3 yrs

[a] Raich (1983).
[b] Hölscher et al. (1998).
[c] Sommer et al. (2003).
[d] Schrott et al. (1999).
[e] Macinnis-Ng et al. (2012).
[f] This study, pre–disturbance situation.
[g] Klinge (1998).
[h] Ubarana (1996).
[i] Lloyd et al. (1988).
[j] Franken et al. (1982).
[k] Cuartas et al. (2007).
[l] Burghouts et al. (1998).
[m] Newbery et al. (1992).
[n] Ewers et al. (2015).
[o] Sinun et al. (1992).
[p] Manfroi et al. (2006).
[q] Asdak et al. (1998b).
[r] Vernimmen et al. (2007).
[s] McJannet et al. (2007).
[#] Stand dominated by *Phenakospermum guyannense.*
[*] Coastal site.
[0] Pre–disturbance situation (cf. Table 9).
[@] Some timber extraction 40 years ago.
[+] Data for year with normal rainfall.
[$] 10 m × 10 m sub–plot with exceptionally large tree.
[$$] 4 ha plot.

characteristics, sampling design, and rainfall regime (e.g. length of dry season; rainfall intensity and duration), certain broad patterns do arise. First, *I*/*P* for very young (1–5 yr) regrowth is generally enhanced the most relative to *I*/*P* in old-growth lowland rain forest, while differences between primary and secondary forest during the next five years of succession or later are already hard to discern. The comparative (short-term) work by Zimmermann et al. (2013) in 16 forest stands in Panamá that ranged between 3 and 30 years of age provides further confirmation that TF/*P*-ratios for forests older than 10 years may not be statistically distinguishable from those for nearby old-growth forest. However, the range reported for their seven 5–7-year-old forests was considerable (87.3–101.6% of *P*). Secondly, stemflow is often much higher in young forests (up to 10 years of age), with an exceptionally high value recorded for 10-year-old regrowth dominated by the banana-like *Phenakospermum* (Hölscher et al., 1998). Overall, there is a dearth of systematic studies in 5–15-year-old forests that include SF- as well as TF measurements over an entire seasonal cycle. Changes in forest structure (notably LAI, tree density, and height) are especially pronounced during the first decade of regrowth (Zimmermann et al., 2013; Scatena et al., 1996) and this is reflected in rapid changes in relative amounts of TF and, especially, SF during this phase (Table 10). Furthermore, most studies to date may well have under-estimated SF by not including the stemflow contributions by (very) small trees and saplings whose funneling ratios are typically high (Manfroi et al., 2004; Honda et al., 2014; González-Martínez et al., 2017). This would seem all the more important for young forests where smaller trees are likely more abundant (Zimmermann et al., 2013; Chazdon, 2014; cf. Supplementary Fig. 1).

5.5. Wet-canopy evaporation rates versus rainfall intensity

For the two periods having more or less fully developed foliage (i.e. periods 1 and 3), TF-based wet-canopy evaporation rates at Manobo (E_{TF}; 0.66–0.70 mm h^{-1}; Table 7) were much higher than E_{PM}-values reported for lowland rain forests elsewhere in the region having similar rainfall amounts and intensities (0.06–0.24 mm h^{-1}; Wallace and McJannet, 2006; Vernimmen et al., 2007). Our pre-disturbance E_{TF} falls in the range of values derived for other South-east Asian lowland rain forests and tree plantations (0.5–0.8 mm h^{-1}; Asdak et al., 1998a; Dykes, 1997; Vernimmen et al., 2007; Waterloo, 1994). Similar discrepancies between E_{PM} and E_{TF} have been reported for many forests and may be attributable to various factors (recently reviewed by Van Dijk et al., 2015), particularly the underestimation of aerodynamic conductance to moisture exchange between the vegetation and the overlying air, g_a (Holwerda et al., 2012), unaccounted horizontal advection of warmer and drier air from nearby areas without rain (Stewart, 1977; Asdak et al., 1998a; Cisneros-Vaca et al., 2018), release of thermal energy stored in the ecosystem itself (especially at the beginning of a storm; Michiles dos and Gielow, 2008; Cisneros-Vaca et al., 2018), and, possibly, larger-scale advection of sensible heat from the ocean in specific settings (Shuttleworth and Calder, 1979; Blyth et al., 1994). Given the modest stature of the Manobo reforest, release of stored thermal energy is less likely to be important, but being situated within 2 km from the Pacific Ocean, lateral transfer of sensible heat from the warm ocean waters off the coast of Leyte cannot be ruled out, especially at night when air temperatures drop below those of seawater (typically 27–29 °C). According to Roberts et al. (2005), a horizontal temperature gradient of 3–4 K per 100 m would be sufficient to sustain a wet-canopy evaporation rate of 0.5 mm h^{-1} (roughly the difference between E_{TF} and E_{PM} at Manobo). Night-time minimum air temperatures measured at the Basper grassland site (3.5 km from Manobo) were around 26.2 °C throughout the year and therefore generally not low enough to reach a 3–4 K difference in temperature between land and sea. Further, drops in air temperature during rainfall were generally small (1.5 °C on average, but occasionally up to 6 °C). This suggests substantial downward (from the air) rather than lateral (from the ocean) transfer of sensible heat to maintain the observed high values of E_{TF} (cf. Stewart, 1977; Blyth et al., 1994; Cisneros-Vaca et al., 2018). Indeed, Holwerda et al. (2012) drew attention to the fact that, on average, values of E_{TF} derived for eight 'oceanic' tropical sites were not enhanced relative to five more 'continental' sites, as had been suggested previously (Shuttleworth and Calder, 1979; Schellekens et al., 1999). Rather, values of E_{TF} tended to be enhanced *within each group* at sites located in dissected or mountainous terrain as opposed to sites situated in less complex terrain (suggesting aerodynamic roughness at the landscape scale to be a key factor), although Holwerda et al. (2012) admitted that a larger comparative data-set would be needed to draw firmer conclusions. No measurements of g_a are available for the study forest but the Manobo ridge is the first topographic rise encountered by moist winds coming from the ocean, suggesting potentially enhanced turbulence and vapour exchange between the forest canopy and the air (Holwerda et al., 2012).

Hourly wet-canopy evaporation rates (E_{TF}) during large and extended storms at Manobo showed a strong and positive relation to hourly rainfall intensity R (Fig. 9). Murakami (2006) found the same phenomenon in a coastal warm-temperate forest in Japan and suggested that this could be caused by enhanced evaporation of fine splash droplets created when high-energy raindrops hit the canopy during intense rainfall. As pointed out by Dunkerley (2009), Dunin et al. (1988) had earlier suggested an effectively similar mechanism, adding that '*turnover of water vapour* [generated in this way] *may be accelerated with increasing rainfall intensity due to an associated increase in the frequency and turbulent intensity of downdrafts*'. Splash impact droplets are produced in large numbers above a threshold R of about 3.4 mm h^{-1} (Dunkerley, 2009), with a doubling of impact velocity causing a tenfold increase in the number of splash droplets (Stow and Stainer, 1977). Rainfall intensities at Manobo exceed 5 mm h^{-1} (i.e. well above the cited 3.4 mm h^{-1} threshold) for about half the time that it rains (Table 5; cf. Zhang et al., 2018a), suggesting a distinct possibility of splash impact droplet generation as well as intensified downdrafts, and thus canopy ventilation. Interestingly, the relationship between hourly E and R at high intensities was steeper for the storm sampled on 10 January 2014 when LAI was low after defoliation by typhoon Haiyan (Figs. 9 and 1a). Since opening of the canopy *reduces* both g_a and the canopy saturation value S (see Section 5.1), the observed steepening of the relationship following defoliation (also reported by Waterloo (1994) but attributed by him to drier post-cyclone conditions; cf. Tanaka et al., 2015) might reflect enhanced production of splash droplets by rain hitting the now exposed branches, as well as enhanced ventilation (Deguchi et al., 2006). Further work could focus on droplet spectra generated on foliated versus defoliated canopies subject to comparable rainfall intensities, and on the effect of high rainfall intensity on added ventilation and mixing of air within the canopy (Dunkerley, 2009; Van Dijk et al., 2015; cf. Dunin et al., 1988). Nevertheless, regardless of the actual mechanism involved, high rates of E will require sufficient amounts of additional sensible heat. As such, there is a distinct need for more information on the changes in temperature and humidity with height above forest canopies (Shuttleworth and Calder, 1979; Blyth et al., 1994; Cisneros-Vaca et al., 2018).

6. Conclusions

Throughfall (TF), stemflow (SF) and rainfall (P) were measured for a year in a coastal 'reforest' (23 years old) at Manobo, Leyte Island, Philippines. The forest was hit by super-typhoon Haiyan in November 2013, which caused extensive defoliation and canopy damage. Nevertheless, leaf area index (LAI) at relatively sheltered mid- and footslope locations recovered more or less to pre-disturbance values after ca. 4 months. Rainfall partitioning was analyzed separately, therefore, for three periods with contrasting canopy conditions, viz. (i) pre-disturbance, (ii) maximum defoliation, and (iii) largely recovered foliage.

Stemflow made up a small percentage of incident P, with weighted mean SF/P ratios of 2.7%, 1.3%, and 2.0% for the respective periods and an overall mean of 2%. Small trees (5–10 cm diameter) contributed 54% (pre-Haiyan) to 63% (post-Haiyan) of all stemflow. Weighted mean throughfall as measured by 24 roving collectors and two large fixed recording gutters for the above data-set varied from 78% of incident precipitation before canopy disturbance to 85% during the period with the most extensive defoliation and 80% after initial foliage recovery. The manually collected TF data exhibited modest cumulative coefficients of variation compared to values reported for several more species-rich old-growth rain forests. Pre-typhoon disturbance values of rainfall interception loss I for the semi-mature Manobo reforest fall in the upper part of the range reported for *old-growth* lowland rain forests in South-east Asia.

The effect of canopy disturbance on annual I at the relatively sheltered mid-slope measurement site was assessed through modeling and appeared to be modest (< 2% of P on an annual basis), although it remains to be seen what the effects would be of repeated and more frequent disturbances of similar magnitude events in future as a result of climatic intensification (cf. Balaguru et al., 2016).

Relative amounts of TF at Manobo were inversely related to LAI during conditions of full foliage but the relation broke down upon canopy disturbance. Moreover, the relationships were strongest for small storms (< 5 mm) and low rainfall intensities (< 5 mm h^{-1}).

Hourly wet-canopy evaporation rates during large and extensive rainfall events were strongly correlated with hourly rainfall intensities and far exceeded values sustained by available radiation. Although horizontal advection of sensible heat from the nearby ocean cannot be excluded, such high evaporation rates are most likely caused by downward advection of sensible heat from the overlying atmosphere. In

addition, high rainfall intensities at Manobo may generate a large number of splash droplets that are more amenable to rapid evaporation.

Acknowledgements

We are grateful to the elders and members of the Manobo Tribe for access to their forest, hospitality and logistical support. Financial support from the China Scholarship Council, VU University Amsterdam, The Netherlands and the Australian Council for International Agricultural Research (ACIAR Grant no. ASEM/2010/050 to J. Herbohn) is gratefully acknowledged. Robert Arandela Magallanes and Robert Dwight helped with the collection of rainfall, stemflow and throughfall data. Thanks are also due to the following ACIAR-project staff for help with the tree inventories: Valentine and Chris Solano, Ray-An Granada, Junrey Moreno, and Ulysses Polea. Cecile-Marie Quiñones M.Sc. and Prof. Victor Asio (Visayas State University) kindly provided soil-related information. We thank Dr. Nestor Gregorio (ACIAR project and University of the Sunshine Coast) for overall facilitation. The complementary and highly constructive comments received from two anonymous reviewers and Dr. T. McVicar substantially improved the manuscript.

Appendix A. Supplementary material

Supplementary data to this article can be found online at https://doi.org/10.1016/j.jhydrol.2018.11.024.

References

Allen, R.G., Pereira, L.S., Raes, D., Smith, M., 1998. Crop evapotranspiration – Guidelines for computing crop water requirements. FAO Irrigation and Drainage Paper 56. Food and Agricultural Organization of the United Nations, Rome.

Ancog, R.C., Florece, L.M., Nicopior, O.B., 2016. Fire occurrence and fire mitigation strategies in a grassland reforestation area in the Philippines. For. Policy Econ. 64, 35–45.

Aquino, A.P., Daquio, C.R.O., 2014. Executive order no. 26: towards a greener Philippines. Policy Paper, Food and Fertilzer Technology Center, Taipei, Taiwan, pp. 10.

Asdak, C., Jarvis, P.G., van Gardingen, P., 1998a. Evaporation of intercepted precipitation based on an energy balance in unlogged and logged forest areas of central Kalimantan. Indonesia. Agric. For. Meteorol. 92, 173–180.

Asdak, C., Jarvis, P.G., van Gardingen, P., Fraser, A., 1998b. Rainfall interception loss in unlogged and logged forest areas of Central Kalimantan. Indonesia. J. Hydrol. 206, 237–244.

Asio, V.B., Jahn, R., Perez, F.O., Navarrete, I.A., Abit, S.M., 2009. A review of soil degradation in the Philippines. Ann. Trop. Res. 31, 69–94.

Balaguru, K., Foltz, G.R., Leung, L.R., Emanuel, K.A., 2016. Global warming-induced upper-ocean freshening and the intensification of super typhoon. Nature Comms. 7, 13670. https://doi.org/10.138/ncomms13670.

Basnet, K., Likens, G.E., Scatena, F.N., Lugo, A.E., 1992. Hurricane Hugo: damage to tropical rain forest in Puerto Rico. J. Trop. Ecol. 8, 47–55.

Beck, H.E., Bruijnzeel, L.A., van Dijk, A.I.J.M., McVicar, T.R., Scatena, F.N., Schellekens, J., 2013. The impact of forest regeneration on streamflow in 12 mesoscale humid tropical catchments. Hydrol. Earth Syst. Sci. 17, 2613–2635.

Blyth, E.M., Dolman, A.J., Noilhan, J., 1994. The effect of forest on mesoscale rainfall: an example from HAPEX-MOBILHY. J. Appl. Meteorol. 33, 445–454.

Boucher, D.H., Vandermeer, J.H., Yih, K., Zamora, N., 1990. Contrasting hurricane damage in tropical rain-forest and pine forest. Ecology 71, 2022–2024.

Bruijnzeel, L.A., Wiersum, K.F., 1987. Rainfall interception by a young *Acacia auriculiformis* (A. Cunn.) plantation forest in West Java, Indonesia: application of Gash's analytical model. Hydrol. Proc. 1, 185–228.

Bruijnzeel, L.A., Eugster, W., Burkard, R., 2005. Fog as a hydrologic input. In: Anderson, M.G. (Ed.), Encyclopedia of Hydrological Sciences. J. Wiley and Sons, Chichester, U.K., pp. 559–582.

Burghouts, T.B.A., van Straalen, N.M., Bruijnzeel, L.A., 1998. Spatial heterogeneity of element and litter turnover in a Bornean rain forest. J. Trop. Ecol. 14, 477–506.

Chandler, D.G., Walter, M.F., 1998. Runoff responses among comon land uses in the uplands of Matalom, Leyte, Philippines. Trans. Amer. Soc. Agric. Eng. 41, 1635–1641.

Chappell, N.A., Bidin, K., Tych, W., 2001. Modelling rainfall and canopy controls on net-precipitation beneath selectively logged tropical forest. Plant Ecol. 153, 215–229.

Chazdon, R.L., 2014. Second Growth: The Promise of Tropical Forest Regeneration in an Age of Deforestation. University of Chicago Press, Chicago, USA.

Chazdon, R.L., Brancalion, P.H.S., Laestadius, L., Bennett-Curry, A., Buckingham, K., Kumar, C., Moll-Rocek, J., Guimarea-Vieria, I.C., Wilson, S.J., 2016. When is a forest a forest? Forest concepts and definitions in the era of forest and landscape restoration. Ambio 45, 538–550.

Chen, Y.Y., Li, M.H., 2016. Quantifying rainfall interception loss of a subtropical broadleaved forest in central Taiwan. Water (Switzerland) 8. https://doi.org/10.3390/w8010014.

Cinco, T.A., de Guzman, R.G., Ortiz, A.M.D., Delfino, R.J.P., Lasco, R.D., Hilario, F.D., Juanillo, E.L., Barba, R., Ares, E.D., 2016. Observed trends and impacts of tropical cyclones in the Philippines. Int. J. Climatol. 36, 4638–4650.

Cisneros-Vaca, C., van der Tol, C., Ghimire, C.P., 2018. The influence of long-term changes in canopy structure on rainfall interception: a case study in speulderbos, the Netherlands. Discuss. Hydrol. Earth Syst Sci. https://doi.org/10.5194/hess-2018-54.

Concepcion, R.N., Samar, E.D., 1995. Grasslands: development attributes, limitations and potentials. In: Bravo, M.V.A., Exconde, A.B. (Eds.), Strengthening Research and Development for Sustainable Management of Grasslands. Forest Research Institute, College, Laguna, The Philippines, pp. 110–116.

Cuartas, L.A., Tomasella, J., Nobre, A.D., Hodnett, M.G., Waterloo, M.J., Múnera, J.C., 2007. Interception water-partitioning dynamics for a pristine rainforest in Central Amazonia: marked differences between normal and dry years. Agric. For. Meteorol. 145, 69–83.

De Gouvenain, R.C., Silander, J.A., 2003. Do tropical storm regimes influence the structure of tropical lowland rain forests? Biotropica 35, 166–180.

Deguchi, A., Hattori, S., Park, H.T., 2006. The influence of seasonal changes in canopy structure on interception loss: application of the revised Gash model. J. Hydrol. 318, 80–102.

Dierick, D., Kunert, N., Köhler, M., Schwendenmann, L., Hölscher, D., 2010. Comparison of tree water use characteristics in reforestation and agroforestry stands across the tropics. In: Tscharntke, T., Leuschner, C., Veldkamp, E., Faust, H., Guhardja, E., Bidin, A. (Eds.), Tropical Rainforests and Agroforests under Global Change. Springer Verlag, Berlin, pp. 293–308.

Dietz, J., Hölscher, D., Leuschner, C., Hendrayanto, 2006. Rainfall partitioning in relation to forest structure in differently managed montane forest stands in Central Sulawesi, Indonesia. For. Ecol. Manage. 237, 170–178.

Dimantala, C.B., Suerte, L.O., Yumul, G.P., Tamayo, R.A., Ramos, E.G.L., 2006. A Cretaceous supra-subduction oceanic basin source for Central Philippine ophiolitic basement complexes: geological and geophysical constraints. Geosci. J. 10, 305–320.

Dunin, F.X., O'Loughlin, E.M., Reyenga, W., 1988. Interception loss from eucalypt forest: lysimeter determination of hourly rates for long term evaluation. Hydrol. Proc. 2, 315–329.

Dunkerley, D.L., 2009. Evaporation of impact water droplets in interception processes: historical precedence of the hypothesis and a brief literature overview. J. Hydrol. 376, 599–604.

Dykes, A.P., 1997. Rainfall interception from a lowland tropical rainforest in Brunei. J. Hydrol. 200, 260–279.

Ewers, R.M., Boyle, M.J.W., Gleave, R.A., Plowman, N.S., Benedick, S., Bernard, H., Bishop, T.R., Bakhtiar, E.Y., Chey, V.K., Chung, A.Y.C., Davies, R.G., Edwards, D.P., Eggleton, P., Fayle, T.M., Hardwick, S., Homathevi, R., Kitching, R., Khoo, M.S., Luke, S.H., March, J.J., Nilus, R., Pfeifer, M., Rao, S.V., Sharp, A.C., Snaddon, J.L., Stork, N., Struebig, M.J., Wearn, O.R., Yusah, K.M., Turner, E.C., 2015. Logging cuts the functional importance of invertebrates in tropical rainforest. Nat. Commun. 6, 6836. https://doi.org/10.1038/ncomms7836.

FAO, 2006. World Reference Base for Soil Resources. World Soil Resources Report no. 103, Food and Agriculture Organization of the United Nations, Rome.

FAO, 2010. Global Forest Resources Assessment 2010. FAO Forestry Paper no. 163. Food and Agricultural Organization of the United Nations, Rome.

FAO, 2016. Global Forest Resources Assessment 2015. How are the world's forests changing? Food and Agricultural Organization of the United Nations, Rome.

Farley, K.A., Jobbággy, E., Jackson, R.B., 2005. Effects of afforestation on water yield: a global synthesis with implications for policy. Global Change Biol. 11, 1565–1576.

Fleischbein, K., Wilcke, W., Goller, R., Boy, J., Valarezo, C., Zech, W., Knoblich, K., 2005. Rainfall interception in a lower montane forest in Ecuador: effects of canopy properties. Hydrol. Proc. 19, 1355–1371.

Førland, E.J., Allerup, P., Dahlström, B., Elomaa, E., Jonsson, T., Madsen, H., Perälä, J., Rissanen, P., Vedin, H., Vejen, F., 1996. Manual for operational correction of Nordic precipitation data. Norwegian Meteorological Institute, Oslo, Norway.

Ford, C.R., Laseter, S.H., Swank, W.T., Vose, J.M., 2011. Can forest management be used to sustain water-based ecosystem services in the face of climate change? Ecol. Applics. 21, 2049–2067.

Franken, W., Leopoldo, P.R., Matsui, E., de Góes Riebeiro, M., 1982. Interception of precipitation in an Amazonian terra firme forest. Suppl. Acta Amaz. 12, 15–22.

Frumau, K.F.A., Burkard, R., Schmid, S., Bruijnzeel, L.A., Tobón, C., Calvo-Alvarado, J.C., 2011. A comparison of the the performance of three types of passive fog gauges under conditions of wind-driven fog and precipitation. Hydrol. Proc. 25, 374–384.

García-Herrera, R., Ribera, P., Hernández, E., Gimeno, L., 2007. Northwest Pacific typhoons documented by Philippine Jesuits, 1566–1900. J. Geophys. Res 112, D06108. https://doi.org/10.1029/2006JD007370.

Garrity, D.P., Soekardi, M., van Noordwijk, M., de la Cruz, R., Pathak, P.S., Gunasena, H.P.M., Van So, N., Huijun, G., Majid, N.M., 1997. The *Imperata* grasslands of tropical Asia: area, distribution, and typology. Agrofor. Syst. 36, 3–19.

Gash, J.H.C., 1979. An analytical model of rainfall interception by forests. Quart. J. Royal Meteorol. Soc. 105 (443), 43–55.

Gash, J.H.C., Morton, A.J., 1978. An application of the Rutter model to the estimation of the interception loss from Thetford Forest. J. Hydrol. 38, 49–58.

Gash, J.H.C., Lloyd, C.R., Lachaud, G., 1995. Estimating sparse forest rainfall interception with an analytical model. J. Hydrol. 170, 79–86.

Ghimire, C.P., Bruijnzeel, L.A., Lubczynski, M.W., Ravelona, M., Zwartendijk, B.W., van Meerveld, H.J., 2017. Measurement and modeling of rainfall interception by two differently aged secondary forests in upland eastern Madagascar. J. Hydrol. 545, 212–225.

González-Martínez, T.M., Williams-Linera, G., Holwerda, F., 2017. Understory and small trees contribute importantly to stemflow in a lower montane cloud forest. Hydrol. Proc. 31, 1174–1183.
Heartsill-Scalley, T., Scatena, F.N., Estrada, C., McDowell, W.H., Lugo, A.E., 2007. Disturbance and long-term patterns of rainfall and throughfall nutrient fluxes in a subtropical wet forest in Puerto Rico. J. Hydrol. 333, 472–485.
Herwitz, S.R., 1986. Infiltration-excess caused by stemflow in a cyclone-prone tropical forest. Earth Surf. Proc. Landforms 11, 401–412.
Holwerda, F., 2005. Water and energy budgets of rain forests along an elevational gradient under maritime tropical conditions. PhD thesis, VU University, Amsterdam, The Netherlands. Available at: http://www.falw.vu.nl/nl/onderzoek/earth-sciences/geo-environmental-science-and-hydrology/hydrology-dissertations/index.asp.
Holwerda, F., Scatena, F.N., Bruijnzeel, L.A., 2006. Throughfall in Puerto Rican lower montane rain forest: a comparison of sampling strategies. J. Hydrol. 327, 592–602.
Holwerda, F., Bruijnzeel, L.A., Scatena, F.N., Vugts, H.F., Meesters, A.G.C.A., 2012. Wet canopy evaporation from a Puerto Rican lower montane rain forest: the importance of realistically estimated aerodynamic conductance. J. Hydrol. 414–415, 1–15.
Hölscher, D., Mackensen, J., Roberts, J.R., 2005. Forest recovery in the humid tropics: changes in vegetation structure, nutrient pools and the hydrological cycle. In: Bonell, M., Bruijnzeel, L.A. (Eds.), Forests, Water and People in the Humid Tropics. Cambridge University Press, Cambridge, U.K., pp. 598–621.
Hölscher, D., Sá de, A.T.D., Möller, R.F., Denich, M., Fölster, H., 1998. Rainfall partitioning and related hydrochemical fluxes in a diverse and in a mono-specific (*Phenakospermum guyannense*) secondary vegetation stand in eastern Amazonia. Oecologia 114, 251–257.
Honda, E.A., Mendonça, A.H., Durigan, G., 2014. Factors affecting the stem flow of trees in the Brazilian Cerrado. Ecohydrology 8, 1351–1362.
Hooper, E., Legendre, P., Condit, R., 2005. Barriers to forest regeneration of deforested and abandoned land in Panama. J. Appl. Ecol. 42, 1165–1174.
Hu, T., Smith, R.B., 2018. The impact of Hurricane Maria on the vegetation of Dominica and Puerto Rico using multispectral remote sensing. Remote Sensing 10 (6), 827.
Jackson, I.J., 1975. Relationships between rainfall parameters and interception by tropical forest. J. Hydrol. 25, 215–238.
Klaassen, W., Bosveld, F., de Water, E., 1998. Water storage and evaporation as constituents of rainfall interception. J. Hydrol. 212–213, 36–50.
Klinge, R., 1998. Wasser- und Nährstoffdynamik im Boden und Bestand beim Aufbau einer Holzplantage im östlichen Amazonasgebiet. Göttinger Beiträge zur Land- und Forstwirtschaft in den Tropen und Subtropen 122, 1–260.
Knutson, T.R., McBride, J.L., Chan, J., Emanuel, K., Holland, G., Landsea, C., Held, I., Kossin, J.P., Srivastava, K., Sugi, M., 2010. Tropical cyclones and climate change. Nature Geosci. 3, 157–163.
Knyazikhin, Y., Glassy, J., Privette, J.L., Tian, Y., Lotsch, A., Zhang, Y., Wang, Y., Morisette, J.T., Votava, P., Myneni, R.B., Nemani, R.R., Running, S. W., 1999. MODIS Leaf Area Index (LAI) and Fraction of Photosynthetically Active Radiation Absorbed by Vegetation (FPAR) Product (MOD15) Algorithm Theoretical Basis Document. Downloaded from: < http://eospso.gsfc.nasa.gov/atbd/modistables.html > .
Kossin, J.P., Emanuel, K.A., Vecchi, G.A., 2014. The poleward migration of the location of tropical cyclone maximum intensity. Nature 509, 349–352.
Krishnaswamy, J., Bonell, M., Venkatesh, B., Purandara, B.K., Lele, S., Kiran, M.C., Reddy, V., Badiger, S., Rakesh, K.N., 2012. The rain-runoff response of tropical humid forest ecosystems to use and reforestation in the Western Ghats of India. J. Hydrol. 472–473, 216–237.
Lacombe, G., Ribolzi, O., de Rouw, A., Pierret, A., Latsachak, K., Silvera, N., Pham Dinh, R., Orange, D., Janeau, J.L., Soulileuth, B., Robain, H., Taccoen, A., Sengpaathith, P., Mouche, E., Sengtaheuanghoung, O., Tran Duc, T., Valentin, C., 2016. Contrasting hydrological impacts of afforestation in the humid tropics evidenced by long-term field monitoring and simulation modelling. Hydrol. Earth Syst. Sci. 20, 2691–2704.
Lamb, D., 1998. Large-scale ecological restoration of degraded tropical forest lands: the potential role of timber plantations. Restor. Ecol. 6, 271–279.
Lasco, R.D., Pulhin, J.M., 2006. Environmental impacts of community-based forest management in the Philippines. Int. J. Environ. Sustain. Dev. 5, 46–56.
Lee, M.F., Lin, T.C., Vadeboncoeur, M.A., Hwong, J.L., 2008. Remote sensing assessment of forest damage in relation to the 1996 strong typhoon Herb at Lienhuachi Experimental Forest, Taiwan. For. Ecol. Manage. 255, 3297–3306.
Lin, T.-C., Hamburg, S.P., Lin, K.-C., Wang, L.-J., Chang, C.-T., Hsia, Y.-J., Vadeboncoeur, M.A., Mabry Mcmullen, C.M., Liu, C.-P., 2011. Typhoon disturbance and forest dynamics: lessons from a Northwest Pacific subtropical forest. Ecosystems 14, 127–143.
Lloyd, C.R., de Marques-Filho, A.O., 1988. Spatial variability of throughfall and stemflow measurements in Amazonian rainforest. Agric. For. Meteorol. 42, 63–73.
Lloyd, C.R., Gash, J.H.C., Shuttleworth, W.J., de Marques-Filho, A.O., 1988. The measurement and modelling of rainfall interception by Amazonian rain forest. Agric. For. Meteorol. 43, 469–485.
Macinnis-Ng, C.M.O., Flores, E.E., Müller, H., Schwendenmann, L., 2012. Rainfall partitioning into throughfall and stemflow and associated nutrient fluxes: land-use impacts in a lower montane tropical region of Panama. Biogeochem. 111, 661–667.
Manfroi, O.J., Koichiro, K., Nobuaki, T., Masakazu, S., Nakagawa, M., Nakashizuka, T., Chong, L., 2004. The stemflow of trees in a Bornean lowland tropical forest. Hydrol. Proc. 18, 2455–2474.
Manfroi, O.J., Kuraji, K., Suzuki, M., Tanaka, N., Kume, T., Nakagawa, M., Kumagai, T., Nakashizuka, T., 2006. Comparison of conventionally observed interception evaporation in a 100-m^2 subplot with that estimated in a 4-ha area of the same Bornean lowland tropical forest. J. Hydrol. 329, 329–349.
McJannet, D., Wallace, J., Reddell, P., 2007. Precipitation interception in Australian tropical rainforests: II. Altitudinal gradients of cloud interception, stemflow, throughfall and interception. Hydrol. Process. 21, 1703–1718.
Michiles dos, S.A.A., Gielow, R., 2008. Above-ground thermal energy storage rates, trunk heat fluxes and surface energy balance in a central Amazonian rainforest. Agric. For. Meteorol. 148, 917–930.
Mulder, C.P.H., Bazeley-White, E., Dimitrakopoulos, P.G., Hector, A., Scherer-Lorenzen, M., Schmid, B., 2004. Species evenness and productivity in experimental plant communities. Oikos 107, 50–63.
Murakami, S., 2006. A proposal for a new forest canopy interception mechanism: Splash droplet evaporation. J. Hydrol. 319, 72–82.
Murniati, 2002. From *Imperata cylindrica* Grasslands to Productive Agroforestry. PhD Thesis. Wageningen University and Research Centre, Wageningen, The Netherlands, pp. 194.
Neal, C., Robson, A.J., Bhardwaj, C.L., Conway, T., Jeffery, T.A., Neal, M., Ryland, G.D., Smith, C.J., Walls, J., 1993. Relationships between precipitation, stemflow, and throughfall for a lowland beech plantation, Black Wood, Hampshire, England: findings on interception at a forest edge and the effects of storm damage. J. Hydrol. 146, 221–233.
Newbery, D.M., Campbell, E.J.F., Lee, Y.F., Ridsdale, C.E., Still, M.J., 1992. Primary lowland dipterocarp forest at Danum Valley, Sabah, Malaysia: structure, relative abundance and family composition. Phil. Trans. Royal Soc. London, Series B 335, 341–356.
Nguyen, P., Sellars, S., Thorstensen, A., Tao, Y.M., Ashouri, H., Braithwaite, D., Hsu, K.L., Sorooshian, S., 2014. Satellites track precipitation of super typhoon Haiyan. EOS 95 (16).
Ohta, S., 1990. Influence of deforestation on the soils of the Pantabangan Area, Central Luzon, the Philippines. J. Soil Sci. Plant Nut. 36, 561–573.
Otsamo, A., Adjers, G., Hadi, T.S., Kuusipalo, J., Vuokko, R., 1997. Evaluation of reforestation potential of 83 tree species planted on Imperata cylindrical dominated grassland—a case study from south Kalimantan. Indonesia. New For. 14 (2), 127–143.
Otsamo, R., 2000. Secondary forest regeneration under fast-growing forest plantations on degraded *Imperata cylindrica* grasslands. New Forests 19, 69–93.
Park, A., Cameron, J.L., 2008. The influence of canopy traits on throughfall and stemflow in five tropical trees growing in a Panamanian plantation. For. Ecol. Manage. 255, 1915–1925.
Pulhin, J.C.M., Chokkalingam, U., Peras, R.J.J., Acosta, R.T., Carandang, A.P., Natividad, M.Q., Lasco, R.D., Rizal, R.A., 2006. Historical overview. In: Chokkalingam, U., Carandang, A.P., Pulhin, J.M., Lasco, R.D., Peras, R.J.J., Toma, T. (Eds.), One century of Forest Rehabilitation in the Philippines. Centre for International Forestry Research, Bogor, Indonesia, pp. 6–41.
Putz, F.E., 1983. Treefall pits and mounds, buried seeds, and the importance of soil disturbance to pioneer trees on Barro Colorado Island, Panama. Ecology 64, 1069–1074.
Rabonza, M.L., Felix, R.P., Lagmay, A.M.F.A., Eco, R.N.C., Ortiz, I.J.G., Aquino, D.T.A., 2015. Shallow landslide susceptibility mapping using high-resolution topography for areas devastated by supertyphoon Haiyan. Landslides. https://doi.org/10.1007/s10346-015-0626-x.
Raich, J.W., 1983. Throughfall and stem flow in mature and year-old wet tropical forest. Trop. Ecol. 24, 234–243.
Roberts, J.M., Gash, J.H.C., Tani, M., Bruijnzeel, L.A., 2005. Controls on evaporation in lowland tropical rainforest. In: Bonell, M., Bruijnzeel, L.A. (Eds.), Forests, Water and People in the Humid Tropics. Cambridge University Press, Cambridge, U.K., pp. 622–650.
Santoso, D., Adiningsih, S., Mutert, E., Fairhurst, T., van Noordwijk, N., 1997. Soil fertility management for reclamation of *Imperata* grasslands by smallholder agroforestry. Agrofor. Syst. 36, 181–202.
Scatena, F.N., Planos-Gutierrez, E.O., Schellekens, J., 2005. Natural disturbances and the hydrology of humid tropical forests. In: Bonell, M., Bruijnzeel, L.A. (Eds.), Forests, Water and People in the Humid Tropics. Cambridge University Press, Cambridge, U.K., pp. 489–512.
Scatena, F.N., Moya, S., Estrada, C., Chinea, J.D., 1996. The first five years in the reorganization of aboveground biomass and nutrient use following Hurricane Hugo in the Bisley experimental watersheds, Luquillo Experimental Forest, Puerto Rico. Biotropica 28, 424–440.
Scatena, F.N., Silver, W., Siccama, T., Johnson, A., Sámchez, M.J., 1993. Biomass and nutrient content of the Bisley watersheds, Luquillo Experimental Forest, Puerto Rico, before and after Hurricane Hugo, 1989. Biotropica 25, 15–27.
Schellekens, J., Scatena, F.N., Bruijnzeel, L.A., Wickel, A.J., 1999. Modelling rainfall interception by a lowland tropical rain forest in northeastern Puerto Rico. J. Hydrol. 225, 168–184.
Schrott, G., Fereira da Silva, L., Wolf, W.A., Texeira, W.G., Zech, W., 1999. Distribution of throughfall and stemflow in multi-strata agroforestry, perennial monoculture, fallow and primary forest in Central Amazonia. Brazil. Hydrol. Proc. 13, 1423–1436.
Scott, D.F., Bruijnzeel, L.A., Mackensen, J., 2005. The hydrological and soil impacts of forestation in the tropics. In: Bonell, M., Bruijnzeel, L.A. (Eds.), Forests, Water and People in the Humid Tropics. Cambridge University Press, Cambridge, U.K., pp. 622–651.
Shuttleworth, W.J., Calder, I.R., 1979. Has the Priestley-Taylor equation any relevance to forest evaporation? J. Appl. Meteorol. 18, 639–646.
Sinun, W., Wong, W., Douglas, I., Spencner, T., 1992. Throughfall, stemflow, overland flow and throughflow in the Ulu Segama rain forest, Sabah, Malaysia. Phil. Trans. Royal Soc. London, Series B 335, 389–395.
Snelder, D.J., 2001. Soil properties of *Imperata* grasslands and prospects for tree-based farming systems in Northeast Luzon, the Philippines. Agrofor. Syst. 52, 27–40.
Snelder, D.J., Lasco, R.D., 2008. Smallholder Tree Growing for Rural Development and Environmental Services. Springer Verlag, Berlin, pp. 494.
Sommer, R., Fölster, H., Vielhauer, K., Carvalho, E.J.M., Vlek, P.L.G., 2003. Deep soil water dynamics and depletion by secondary vegetation in the eastern Amazon. Soil Sci. Soc. Am. J. 67, 1672–1686.

Stewart, J.B., 1977. Evaporation from the wet canopy of a pine forest. Water Resourc. Res. 13, 915–921.
Stow, C.D., Stainer, R.D., 1977. The physical products of a splashing water drop. J. Meteorol. Soc. Jap. 55, 518–532.
Styger, E., Rakotondramasy, H.M., Pfeffer, M.J., Fernandes, E.C.M., Bates, D., 2007. Influence of slash-and-burn farming practices on fallow succession and land degradation in the rainforest region of Madagascar. Agric. Ecosyst. Environ. 119, 257–269.
Tanaka, N., Levia, D., Igarashi, Y., Nanko, K., Yoshifuji, N., Tanaka, K., Tantasirin, C., Suzuki, M., Kumagai, T., 2015. Throughfall under a teak plantation in Thailand: a multifactorial analysis on the effects of canopy phenology and meteorological conditions. Int. J. Biometeorol. 59, 1145–1156.
Tanaka, N., Levia, D., Igarashi, Y., Yoshifuji, N., Tanaka, K., Tantasirin, C., Nanko, K., Suzuki, M., Kumagai, T., 2017. What factors are most influential in governing stemflow production from plantation-grown teak trees? J. Hydrol. 544, 10–20.
Teklehaimanot, Z., Jarvis, P.G., Ledger, D.C., 1991. Rainfall interception and boundary layer conductance in relation to tree spacing. J. Hydrol. 123, 261–278.
Thom, A.S., 1975. Momentum, mass and heat exchange of plant communities. In: Monteith, J.L. (Ed.), Vegetation and the Atmosphere, 1. Academic Press, London, Principles, pp. 57–109.
Ubarana, V.N., 1996. Observations and modelling of rainfall interception at two experimental sites in Amazonia. In: Gash, J.H.C., Nobre, C.A., Roberts, J.M., Victoria, R.L. (Eds.), Amazonian Deforestation and Climate. J. Wiley, Chichester, U.K., pp. 151–162.
Van Dijk, A.I.J.M., Bruijnzeel, L.A., 2001. Modelling rainfall interception by vegetation of variable density using an adapted analytical model. Part 1. Model description. J. Hydrol. 247, 230–238.
Van Dijk, A.I.J.M., Gash, J.H.C., van Gorsel, E., Blanken, P.D., Cescatti, A., Emmel, C., Gielen, B., Harman, I.N., Kiely, G., Merbold, L., Montagnani, L., Moors, E., Sottocornola, M., Varlagin, A., Williams, C.A., Wohlfahrt, G., 2015. Rainfall interception and the coupled surface water and energy balance. Agric. For. Meterol. 214–215, 402–415.
Vernimmen, R.R.E., Bruijnzeel, L.A., Romdoni, A., Proctor, J., 2007. Rainfall interception in three contrasting lowland rain forest types in Central Kalimantan, Indonesia. J. Hydrol. 340, 217–232.
Walker, L.R., 1991. Tree damage and recovery from Hurricane Hugo in Luquillo Experimental Forest, Puerto Rico. Biotropica 23, 379–385.
Wallace, J., McJannet, D., 2006. On interception modelling of a lowland coastal rainforest in northern Queensland, Australia. J. Hydrol. 329, 477–488.
Wallace, J.S., McJannet, D., 2008. Modelling interception in coastal and montane rainforests in northern Queensland, Australia. J. Hydrol. 348, 480–495.
Walsh, R.P.D., 1996. Climate. In: Richards, P.W. (Ed.), The Tropical Rain Forest, second ed. Cambridge University Press, Cambridge, U.K., pp. 159–205.
Waterloo, M.J., 1994. Water and nutrient dynamics of Pinus caribaea plantation forests on former grassland soils in Viti levu, Fiji. PhD thesis, VU University, Amsterdam, The Netherlands. Available at: < http://www.falw.vu.nl/nl/onderzoek/earth-sciences/geo-environmental-science-and-hydrology/hydrology-dissertations/index.asp >.
Waterloo, M.J., Bruijnzeel, L.A., Vugts, H.F., Rawaqa, T.T., 1999. Evaporation from *Pinus caribaea* plantations on former grassland soils under maritime tropical conditions. Water Resourc. Res. 35, 2133–2144.
Wills, J., Herbohn, J., Maranguit Moreno, M.O., Avela, M.S., Firn, J., 2016. Next-generation tropical forests: reforestation type affects recruitment of species and functional diversity in a human-dominated landscape. J. Appl. Ecol. https://doi.org/10.1111/1365-2664.12770.
Wishnie, M.H., Dent, D.H., Mariscal, E., Deago, J., Cedeño, N., Ibarra, D., Condit, R., Ashton, P.M.S., 2007. Initial performance and reforestation potential of 24 tropical tree species planted across a precipitation gradient in the Republic of Panamá. For. Ecol. Manage. 243, 39–49.
Yao, A.W., Chiang, J.M., McEwan, R., Lin, T.C., 2015. The effect of typhoon-related defoliation on the ecology of gap dynamics in a subtropical rain forest of Taiwan. J. Veg. Sci. 26, 145–154.
Zhang, J., Bruijnzeel, L.A., Quiñones, C.M., Tripoli, R., Asio, V.B., van Meerveld, H.J., 2018a. Soil physical characteristics of a degraded tropical grassland and a 'reforest': implications for runoff generation. Geoderma 333, 163–177.
Zhang, J., van Meerveld, H.J., Tripoli, R., Bruijnzeel, L.A., 2018b. Runoff response and sediment yield of a landslide-affected fire-climax grassland catchment (Leyte, The Philippines) before and after passage of typhoon Haiyan. J. Hydrol. 565, 524–537.
Zhou, G.Y., Wei, X., Luo, Y., Zhang, M., Li, Y., Qiao, Y., Liu, H., Wang, C., 2010. Forest recovery and river discharge at the regional scale of Guangdong Province. China. Water Resour. Res. 46, W09503. https://doi.org/10.1029/2009WR 008829.
Ziegler, A.D., Bruun, T.B., Guardiola-Claramonte, M., Giambelluca, T.W., Lawrence, D., Thanh Lam, N., 2009. Environmental consequences of the demise in swidden cultivation in montane mainland Southeast Asia: hydrology and geomorphology. Human Ecol. 37, 361–373.
Zimmerman, J.K., Everham, E.M., Waide, R.B., Lodge, D.J., Taylor, C.M., Brokaw, N.V.L., 1994. Response of tree species to hurricane winds in subtropical wet forest in Puerto Rico: implications for tropical tree life histories. J. Ecol. 82, 911–922.
Zimmermann, A., Uber, B., Zimmermann, B., Elsenbeer, H., 2015. Predictability of stemflow in a species-rich tropical forest. Hydrol. Proc. 29, 4947–4956.
Zimmermann, B., Zimmermann, A., Scheckenbach, H.L., Schmid, T., Hall, J.S., van Breugel, M., 2013. Changes in rainfall interception along a secondary forest succession gradient in lowland Panama. Hydrol. Earth Syst. Sci. 17, 4659–4670.